

Trajectories of land and ocean primary productivity across the Arctic coastal margin and sensitivity to coastal sea ice decline

Cynthia Garcia^{1,2}, Max Berkelhammer³, and Larry Stock³

¹Department of Earth, and Environmental Sciences, University of Illinois at Chicago

²National Oceanic and Atmospheric Administration

³Affiliation not available

August 25, 2023

Abstract

The rapidly warming Arctic and its effects on sea ice extent, hydrology, and nutrient availability influence terrestrial and marine carbon cycles in a number of interrelated ways. While these changes likely have shared effect on adjacent land and ocean systems, we often study them in isolation, making it difficult to understand response patterns and trajectories in these carbon cycle hotspots. Using almost two decades of remotely-sensed Gross Primary Productivity (GPP) in Arctic coastal margins, we test how the magnitude and direction of change in productivity covary. We observed that coastal marine productivity is four times that of coastal tundra productivity in the pan-Arctic. From 2003-2020, GPP in both the coastal land and ocean increased by approximately 12%. This common trajectory seems to be a product of increasing open water conditions, increased terrestrial water balance, and nutrient availability as driven by the regional warming. On a sectoral scale, we proposed a Coastal Synchrony Index (CSI) to compare the rate of change of ocean productivity relative to land productivity and show that ocean productivity is increasing faster than land in *inflow margins* of Barents, Bering, and Okhotsk, *outflow margins* of Canadian Arctic Archipelago (CAA) and Greenland/Iceland, and in *interior margin* of Eurasia. Additionally, we see strong coherence between land and ocean GPP on 4–5-year cycles illustrating that coastal synchrony observed over decadal timescales is mirrored over interannual timescales. These cycles align with variations in open water duration, emphasizing the pivotal role of reducing shorefast ice on terrestrial and marine productivity trajectories.

This is a preprint and has been submitted for peer review.

1 **Trajectories of land and ocean primary productivity across the Arctic coastal margin and**
2 **sensitivity to coastal sea ice decline**

3
4 Cynthia Garcia^{1,2}

5 ceidel2@uic.edu, cynthia.garcia@noaa.gov

6 Max Berkelhammer¹

7 berkelha@uic.edu

8 Larry Stock⁻³

9 larry.v.stock@nasa.gov

10
11 ¹University of Illinois at Chicago, Department of Earth, and Environmental Sciences,
12 Chicago, IL, 60607 USA, ²National Oceanic and Atmospheric Administration, Silver Spring,
13 MD 20910, USA, ³Insight Global, Arlington, VA 22209, USA

14
15 Corresponding author: Cynthia Garcia (ceidel2@uic.edu)

16
17 **Key Points:**

- 18 • From 2003-2020, coastal land and ocean GPP increased by the same magnitude of 12%
19 and is displaying a *Synchronized Positive Shift (SPS)*.
- 20 • This converging response seems to be a product of increasing open water conditions and
21 water and nutrient availability as driven by general warming.
- 22 • Land and ocean GPP show strong synchrony over 4–5-year cycles, illustrating that coastal
23 synchrony observed over decadal timescales is mirrored over interannual timescales.

24
25 **Abstract**

26
27 The rapidly warming Arctic and its effects on sea ice extent, hydrology, and nutrient availability
28 influence terrestrial and marine carbon cycles in a number of interrelated ways. While these
29 changes likely have shared effect on adjacent land and ocean systems, we often study them in
30 isolation, making it difficult to understand response patterns and trajectories in these carbon cycle
31 hotspots. Using almost two decades of remotely-sensed Gross Primary Productivity (GPP) in

32 Arctic coastal margins, we test how the magnitude and direction of change in productivity covary.
33 We observed that coastal marine productivity is four times that of coastal tundra productivity in
34 the pan-Arctic. From 2003-2020, GPP in both the coastal land and ocean increased by
35 approximately 12%. This common trajectory seems to be a product of increasing open water
36 conditions, increased terrestrial water balance, and nutrient availability as driven by the regional
37 warming. On a sectoral scale, we proposed a Coastal Synchrony Index (CSI) to compare the rate
38 of change of ocean productivity relative to land productivity and show that ocean productivity is
39 increasing faster than land in *inflow margins* of Barents, Bering, and Okhotsk, *outflow margins* of
40 Canadian Arctic Archipelago (CAA) and Greenland/Iceland, and in *interior margin* of Eurasia.
41 Additionally, we see strong coherence between land and ocean GPP on 4–5-year cycles illustrating
42 that coastal synchrony observed over decadal timescales is mirrored over interannual timescales.
43 These cycles align with variations in open water duration, emphasizing the pivotal role of reducing
44 shorefast ice on terrestrial and marine productivity trajectories.

45

46 **1. Introduction**

47

48 The rapid declines in Arctic sea ice extent, melting permafrost, warming, and changes in hydrology
49 are influencing Arctic land and ocean carbon cycles in a number of interrelated ways (Irrgang et
50 al., 2022; Post et al., 2013; Schuur et al., 2015; Carmack et al., 2015; Rawlins et al., 2010). While
51 a changing cryosphere and longer ice-free growing season would likely have a shared influence
52 on land and ocean productivity, we often study them in silos. Consequently, their long-term joint
53 behavior is generally poorly understood despite the numerous ways that coastal land and ocean
54 systems are affected by similar mechanisms. On the ocean side, dramatic increases in ice-free areas
55 have been shown to positively affect phytoplankton primary production in the open ocean (Lewis
56 et al., 2020). Increasing wind mixing from more frequent storms has also been ascribed to promote
57 the resuspension and upwelling of nutrients to the euphotic zone (Zhang et al., 2010; Tremblay et
58 al., 2015). At the same time, increasing surface ocean stratification due to the intensification of
59 freshwater flux from river runoff, ice melt, and positive precipitation minus evaporation (P-E) can
60 limit ocean primary productivity due to its control on the transfer of nutrients to the surface layers
61 (Nummelin et al. 2016; McLaughlin & Carmack, 2010, Popova et al., 2012). With a continued

62 decrease in sea ice cover, a cloudier, wetter Arctic is also expected (Liu et al., 2012; McIlhatten,
63 et al., 2020), which can reduce surface ocean primary production.

64

65 On the terrestrial side, observations across various spatial scales show both greening and browning
66 trends across the Arctic (Bhatt et al., 2010; Epstein et al., 2018). The presence of these diverging
67 trends reflects a combination of co-occurring processes including increases in precipitation (that
68 can aid water-limited systems but also lead to water-logging), higher CO₂ and nutrient deposition
69 (fertilization), warmer temperatures (2-4 times the global average rate) (Rantanen et al., 2022;
70 England et al., 2021), and higher evaporative demand as well as novel biotic interactions such as
71 shrub encroachment and pests (Kankaanpää, et al., 2020). These changes in tundra vegetation
72 have critical impacts on coastal permafrost stability, hydrologic cycles, and the exchange of
73 materials between land and ocean, leading to major changes in the biogeochemical cycling in both
74 land and ocean systems.

75

76 Limited studies have focused on understanding the large-scale variability of adjacent land and
77 ocean carbon cycle across the radically changing Arctic coast. As the site of major exchange of
78 water and other materials, strong connections between near-shore marine ecosystems and coastal
79 tundra productivity are expected. Additionally, most of the Arctic tundra biome is closely tied to
80 the adjacent marine system because about 80% of it is within 100 km of the coastline (Walker et
81 al., 2005; Minke et al., 2007). To provide a regional view of the heterogeneity and coherency in
82 coastal carbon cycle changes, we assess concurrent estimates of gross primary production (GPP),
83 i.e., total fixation of carbon by primary producers through photosynthesis along adjacent land and
84 ocean systems. Since ground-based and in-situ estimates of primary production are sparse in the
85 Arctic, especially along coastal areas, this study takes advantage of the inherent ability of remote
86 sensing datasets to provide long-term continuous observations that cross both the land and ocean
87 interface. Here, we present a generalized coastal trajectory classification scheme based on
88 observed temporal primary productivity trends in adjacent land and ocean systems. Moreover, land
89 and ocean GPP are also dependent on a complex collection of factors, most notably light
90 availability (Leu et al., 2015; Frey et al., 2011), nutrients (Tremblay et al., 2015; Fernandez-
91 Mendez et al., 2015), temperature (Bhatt et al., 2013), water limitations (Elmendorf et al., 2012),
92 and the influence of large-scale teleconnections (Slagstad et al., 2011; Bhatt et al., 2010).

93 Understanding the covariability of these important parameters with primary production could
94 elucidate the links and the nature of coherency between adjacent land and ocean, which can
95 contribute to understanding the way Earth System models capture complex cross-system
96 dynamics.

97
98 The Arctic coastal margins are also highly sensitive to the presence or absence of sea ice. We
99 expect a strong link between coastal sea ice and productivity since shorefast ice provides a first-
100 order control on the physical vulnerability of the coast to erosion and inundation (Barnhard et al.,
101 2014). Shorefast ice is an important buffer from wave action and temperature for considerable
102 portions of the year (Farquharson, et al., 2018), and thus affects the amount of energy available for
103 coastal primary production. With the rapidly declining sea ice extent (with 2020 sea ice minima
104 being the second lowest after 2012) (NSIDC, 2020) and increasing frequency and duration of warm
105 winter air temperature events (Graham et al., 2017), it is anticipated that such changes will have
106 significant ecological consequences. Assessing the simultaneous impact of decreasing coastal sea
107 ice on productivity across the land and ocean interface is therefore necessary not just to understand
108 land-ocean primary productivity trajectory and patterns, but to also help answer questions on how
109 the coastal margins will evolve in a new Arctic climate. To analyze this, we investigate key factors
110 that might be able to explain regional land-ocean GPP coherence. Ultimately, by characterizing
111 these important yet largely unknown connections along the Arctic coastal interface and related
112 feedbacks, we hope to better inform biogeochemical processes and models, especially in the face
113 of accelerating rates of Arctic terrestrial carbon cycling (Jeong et al., 2018) and ice-free summers
114 now projected in 2030 (Kim et al., 2023).

115

116 **2. Data and Methods**

117

118 ***2.1. Coastal Trajectory Assessment***

119

120 Here, we analyze almost two decades of primary productivity data that are concurrently available
121 over land and ocean in the Arctic. We use FluxSat v2.0 GPP product (Joiner & Yoshida, 2020)
122 over land, which is based on a light-use efficiency model and trained using in-situ eddy covariance
123 measurements. FluxSat is based on the MCD43C Bidirectional Reflectance Distribution Function

124 (BRDF)-Adjusted reflectance from the Moderate-resolution Imaging Spectroradiometer (MODIS)
125 Terra and Aqua. Apart from providing daily gridded estimates of GPP at 0.05-degree resolution,
126 FluxSat v2.0 has observations from March 2000 to present, providing valuable insights into trends
127 and changes in GPP over time. The GPP on the ocean side is estimated from three distinct data
128 products. The first one developed by Lewis & Arrigo (2020) (herein referred to as Lewis) was
129 created to account for the unique bio-optical properties of Arctic waters. The Lewis daily gridded
130 NPP data (with units of $\text{mg C m}^{-2} \text{ d}^{-1}$) are available at four (4) km resolution from 2003 to 2020.
131 Other global ocean Net Primary Productivity (NPP) estimates available are through the ocean
132 productivity products of the Oregon State University available at either ~ 9 km (1080 x 2160 global
133 grid) or ~ 18 km (2160 x 4320 global grid) spatial resolution from July 2002 to present. Data used
134 here include the Vertically Generalized Production Model (VGPM) (Behrenfeld & Falkowski,
135 1997) and the Carbon-based Productivity Model (CbPM) (Westberry et al., 2008). The Lewis NPP
136 data was estimated using updated chlorophyll-a concentration developed by using 501 concurrent
137 measurements of in situ remote sensing reflectance and chlorophyll-a, gathered from 25 distinct
138 cruises across the Arctic Ocean (Lewis, et al., 2020). The VGPM product utilizes a widely used
139 algorithm for estimating ocean NPP at regional to global scales. It is based on the relationship
140 between NPP and chlorophyll-a concentration in the water, and calculates NPP as a product of
141 chlorophyll-a, maximum daily net primary production per unit of chlorophyll in a given water
142 column, day length, and a volume function that accounts for the decreasing photosynthetic rates
143 with depth due to light penetration. Lastly, the CbPM algorithm relates NPP with phytoplankton
144 carbon biomass (estimated from particulate backscattering coefficients) and growth rates
145 (estimated from chlorophyll-to-carbon ratios). The CbPM also estimates a spectrally-resolved
146 attenuation of light through the euphotic zone, providing an estimate of light available for
147 photosynthesis. To estimate GPP from the three ocean NPP products, we use a conversion factor
148 based on empirical characterization of phytoplankton photosynthetic efficiency, wherein GPP was
149 found to be 3.3 times greater than NPP (Halsey et al., 2010).

150

151 All of the land and ocean GPP products are presented with the common unit of $\text{g C m}^{-2} \text{ d}^{-1}$ and are
152 gridded on the same SSM/I (Special Sensor Microwave/Imager) polar stereographic grid with 12.5
153 km spatial resolution using a drop-in-the-bucket binning procedure (Kwok, 2022; Jensen, 2006)
154 on a monthly basis. All monthly primary productivity data from 2003 to 2020 that fall within 100

155 km of a coastline across the pan-Arctic are extracted using the Distance to the Nearest Coastline
 156 dataset of NASA (NASA OBP & Stumpf, 2012). The choice of using a 100-km nearshore buffer
 157 is because the global average of the width of continental shelves ranges from about 50-100 km
 158 (Harris et al., 2014). Shelf seas are areas of extensive deposition due to their proximity to river
 159 systems that supply sediments to the continental margins. With this spatial extent, we assume to
 160 capture processes occurring within Arctic tidal rivers, tidal wetlands, estuaries, and continental
 161 shelves and highlight the signals influenced by land- and marine-derived materials and energy
 162 flow across the coastal interface (Ward et al., 2020). On land, we look at the same 100-km buffer
 163 to ensure that we are looking at similar areas adjacent to the shoreline. This area can provide
 164 primary production along permafrost-affected coasts upstream from estuaries. These transition
 165 zones, affected by both terrestrial and marine influences, possess distinct characteristics. By
 166 analyzing the 100-km strip on both sides of the coastline, we gain a comprehensive perspective of
 167 how terrestrial factors impact marine processes and vice versa. Additionally, our examination of
 168 GPP seasonality revealed that the selected spatial extent remains largely consistent, even when
 169 considering thresholds between 50 and 100 km.

170
 171 To address the heterogeneity
 172 across the Arctic coastlines, we
 173 divided the study area into nine
 174 (9) sectors based on ocean
 175 basins (Comiso, 2015) and
 176 analyzed them separately.
 177 These sectors are shown in
 178 figure 1 and labeled as
 179 Eurasian, Amerasian, Bering,
 180 Barents, Canadian Arctic
 181 Archipelago (CAA),
 182 Baffin/Labrador (B/L),
 183 Greenland/Iceland (G/I),
 184 Hudson Bay, and Okhotsk. The

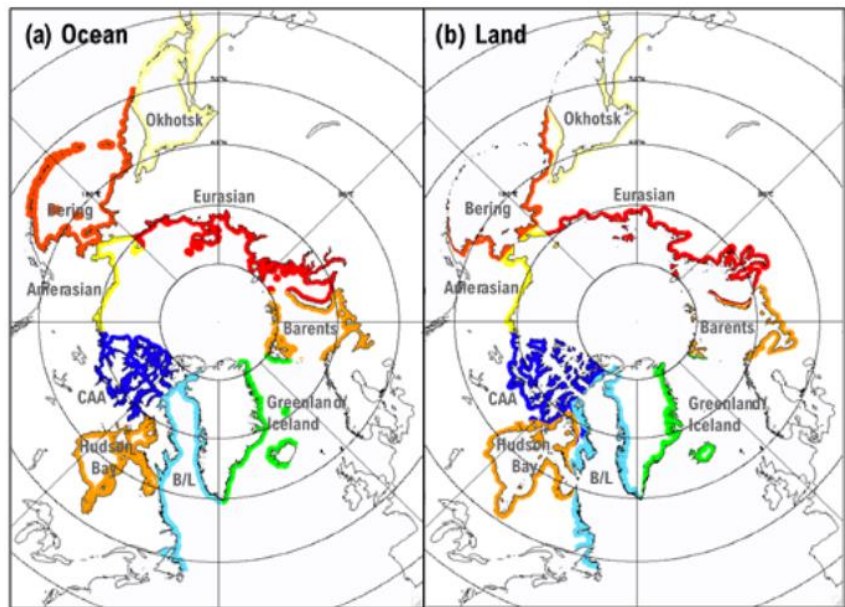


Figure 1. Nine Arctic coastal sectors. Color-coded areas represent the 100-km spatial extent from the coastline towards the (a) ocean and (b) land where data are collected. The nice sectors are Okhotsk, Bering, Eurasian, Barents, Greenland/Iceland, B/L, Hudson Bay, CAA, and Amerasian sectors (Comiso, 2015).

185 color-coded shaded areas represent the 100-km spatial extent from the coastline towards the ocean

186 and towards land. The Eurasian sector covers the coastal regions along East Siberian, Laptev, and
187 Kara Seas and is characterized by diverse Arctic ecosystems, including tundra, boreal forests, and
188 coastal wetlands. The Eurasian sector experiences significant freshwater runoff from major Arctic
189 rivers including the Ob, Yenisey, and Lena (Jakobsson, 2002). The Amerasian encompasses the
190 coastal areas along North America and features tundra, taiga, and coastal plains. This region is
191 dominated by the Beaufort Sea. It is impacted by the inflow of nutrient-rich waters from the Pacific
192 Ocean and the large Mackenzie River (Carmack, E., et al., 2016). The Bering sector corresponds
193 to the coastal regions around the Bering Sea, an area rich in marine biodiversity. The mixing of
194 Pacific and Arctic waters in the Bering Sea creates a productive environment supporting a variety
195 of marine life. Barents sector includes coastal areas along the Barents Sea and off the northern
196 coasts of Norway and Russia. It is an important area for commercial fisheries and a site for the
197 mixing of warm Atlantic water with colder Arctic water. Its coastline also experiences
198 considerable reductions in sea ice cover from recent warming (Isaksen et al., 2022). The Canadian
199 Arctic Archipelago (CAA) is a sector characterized by a series of large island groups in Northern
200 Canada. It contains one-third of the global volume of land ice outside of Greenland and Antarctic
201 ice sheets (Radic' & Hock, 2010). The Baffin/Labrador (B/L) sector includes the Baffin Bay and
202 Labrador Sea, both notable for their interactions between glaciers and ocean currents. These waters
203 are major sinks for atmospheric CO₂ being a region for deep water formation and primary
204 production (DeGrandpre et al., 2006). The Greenland/Iceland (G/I) sector is characterized by its
205 massive ice sheet in Greenland and meltwater coming from it as well as the volcanic landscapes
206 of Iceland. Located in northeastern Canada, the Hudson Bay sector is a large inland sea connected
207 to the Atlantic Ocean via the Hudson Strait. It is characterized by its seasonal ice cover and high
208 freshwater input from large rivers. Lastly, the Okhotsk sector is off the coast of Russia's far east,
209 separated from the Pacific by the Kuril Islands. The sector is notable for sea ice production, which
210 drives ocean circulation and biogeochemical cycles (Nishioka et al., 2014).

211
212 We utilize a generalized coastal trajectory classification scheme based on observed temporal
213 primary productivity trends in adjacent land and ocean systems. We call a coastal region with
214 positive trends in both land and ocean primary productivity an area experiencing *Synchronized*
215 *Positive Shift (SPS)*. For this classification, it is hypothesized that the same changes (e.g., warmer
216 temperature, more rain, increased coastal open water days, and less snow) are positively affecting

217 both systems. For areas with both land and ocean primary productivity decreasing with time, we
218 classify them as *Synchronized Negative Shift (SNS)* areas. In this scenario, common changes in sea
219 ice cover, temperature, and water availability are negatively impacting both systems. This can
220 emerge from factors such as higher evaporative demand leading to water stress for land plants and
221 loss of habitat for primary producers in the sea ice. Areas with heavy and constant coastal erosion
222 can also cause land GPP to decrease as well as carry particles and colored dissolved organic matter
223 (cDOM) to adjacent marine systems that can cause increased turbidity, lessening ocean GPP. For
224 conditions where land productivity is increasing while ocean productivity is decreasing or vice
225 versa, it suggests a divergence in the trends. For the opposing trajectories, we have *Terrestrial-*
226 *Dominant Shift (TDS)* and *Marine-Dominant Shift (MDS)*. We characterize *TDS* as the scenario
227 when land GPP increases, while ocean GPP decreases. Here, the same factors can cause opposite
228 effects on adjacent systems. For example, warmer temperatures and more moisture can cause
229 increases in land GPP. On the ocean side, however, warmer SST and increased freshwater flux
230 from major Arctic rivers can cause lower ocean GPP with time due to stratification-induced
231 nutrient limitation despite enhanced light transmission. For the *MDS* classification, ocean GPP
232 increases while land GPP decreases. This can potentially occur due to increasing frequency of
233 Arctic storms (Clow et al., 2011) that carry high winds and large amounts of rain that can
234 potentially negatively affect land GPP through water-logging. Arctic storms are also most active
235 in summer (Day & Hodges, 2018), which could reduce light availability and reduce GPP. On the
236 ocean side, increasing windiness can potentially promote vertical mixing in the ocean and erode
237 stratification, potentially promoting the upward delivery of new nutrients to the depleted euphotic
238 zone as well as instigating secondary blooms in autumn. Strong winds can also expedite the
239 breakup of sea ice, expanding the available open water area for photosynthesis. Lastly, we have
240 the *No Change* scenario where neither land nor ocean are changing. Here, GPP remains constant
241 and does not change with time. Apart from a generalized coastal trajectory classification scheme,
242 we further categorize the sectors as either an *Interior margin* (Eurasian and Amerasian), which are
243 coastal margins that are mostly influenced by the major Arctic rivers; *Inflow margin* (Bering,
244 Okhotsk, and Barents), which are areas that are influenced by the inflow of warm, salty waters
245 from the Pacific and Atlantic; and *Outflow margin* (CAA, B/L, G/I, and Hudson Bay), which are
246 mostly influenced by cold, fresh water outflows from the Arctic Ocean (Carmack et al., 2006).

247 Annual and monthly aggregated time series for each sector were calculated and trends from
248 monthly anomalies were determined using linear regression. The slope of the regression is
249 considered significant for p values <0.05 . Trends and total percent change for data from April to
250 September (ice-free, productive periods on both land and ocean) from the years 2003-2020 are
251 presented. On the ocean side, we only estimate GPP from open water areas or those with $<15\%$
252 sea ice concentration, and thus exclude primary production under or on sea ice. The 15% threshold
253 is a standard definition used by the National Snow and Ice Data Center (NSIDC) to distinguish
254 between ice-covered and ice-free areas (NSIDC, 2021). Spatial trends and estimates of land and
255 ocean GPP from multi-year average in gC d^{-1} from 100 km landward and oceanward from the
256 coastline in the Pan-Arctic (all coastal margins found at $>60^\circ\text{N}$) are also presented. The months of
257 peak primary productivity from the long-term dataset are also extracted to assess and compare
258 seasonal variability and shifts in peak productivity on adjacent land and ocean domains. To
259 evaluate coastal trajectory, we follow our proposed generalized classification scheme based on
260 observed long-term primary productivity trends.

261

262 *2.2. Coastal Trajectory Mechanisms*

263

264 To investigate factors that might influence the observed Arctic coastal patterns of productivity, we
265 assess the anomaly trends of key remotely sensed parameters that affect both land and ocean during
266 the same study period. These include Land Surface Temperature (LST) -from the MODIS Aqua
267 MYD11C3 version 6 data product (Wan et al., 2021), precipitation minus evaporation (P-E), runoff
268 over land, P-E over the ocean, and upwelling favorable wind days from the European Centre for
269 Medium-Range Weather Forecasts (ECMWF) Reanalysis 5 (ERA5) (Muñoz-Sabater, 2019).
270 Upwelling favorable wind conditions were also assessed by looking at the number of days during
271 the study period when winds were east/northeast parallel to the shelf break, and if alongshore wind
272 speeds exceeded 5 m/s (Cury & Roy, 1989; Bakun, 1990). We assessed the number of open-water
273 (OW) days using the Bootstrap version 2 (SB2) sea ice concentration data (Comiso et al., 2017)
274 from the NSIDC. The duration of OW is defined here as the average number of days where the
275 pixels are ice-free ($<15\%$ sea ice concentration). For consistency with the land and ocean primary
276 productivity data sets used in this study, all temperature, P-E, OW days, and sea ice products were
277 also gridded in the same polar stereographic grid with 12.5 km resolution on a monthly basis.

278

279 We focus on changes in temperature, water availability, coastal sea ice conditions, and upwelling
280 favorable wind days because these are key essential variables that affect both land and ocean
281 systems on our time scale of interest. Temperature affects the metabolic rates of photosynthesizing
282 organisms (both terrestrial plants and marine phytoplankton), influencing their growth rates and,
283 consequently, primary productivity (Clarke & Gaston, 2006). On land, water availability directly
284 impacts plant growth and productivity (Rodriguez-Iturbe, 2000). In the ocean, freshwater inputs
285 from rivers or melting sea ice can affect the stratification of the water column, nutrient availability,
286 and light penetration, all of which can influence phytoplankton productivity (Garcia, et al., 2021;
287 Arrigo & van Dijken, 2004). Coastal sea ice and OW conditions affect light availability for
288 phytoplankton growth and influence nutrient dynamics by its seasonal melting and freezing
289 processes (Leu et al., 2015). These three variables are also interconnected and can influence each
290 other, resulting in compounded effects on coastal primary productivity (Post et al., 2009). Just like
291 with the coastal trajectory assessment of primary productivity, the temperature, water availability,
292 OW conditions as well as upwelling favorable wind days were evaluated using data from 2003-
293 2020 within the 100 km from the coastline to land and ocean from the pan-Arctic (>60°N) and the
294 nine sectors. Other variables analyzed were instantaneous nutrient export from major Arctic river
295 monitoring gauges. We acknowledge that in the surface ocean, primary production is limited by
296 the availability of key nutrients such as nitrogen, phosphorus, and iron. While this is important,
297 data available on a regional scale are scarce and are limited to point measurements typically around
298 the mouths of major Arctic rivers making the characterization of nutrient limitations challenging.
299 It is worth noting, however, that although we did not directly assess nutrients, we used indicators
300 like runoff and upwelling as proxies to infer nutrient limitation on GPP.

301

302 To compare changes in land-ocean primary productivity with changes in temperature, water
303 availability, and coastal OW conditions we estimate a Coastal Synchrony Index (CSI). The CSI is
304 defined here as the quotient of the rate of change in ocean GPP over the rate of change in land GPP
305 for each of the sectors. This ratio represents the rate of change of ocean productivity relative to the
306 rate of change of land productivity and can offer insights into how marine and terrestrial
307 productivity are related. If the CSI is greater than 1, it suggests ocean productivity is changing at
308 a faster rate than land productivity. If the ratio is less than 1, it indicates that ocean productivity is

309 changing at a slower rate than land productivity. A ratio of 1 implies that both are changing at the
310 same rate. The CSI can be a valuable metric in understanding the relative dynamics of change
311 between land and ocean productivity, potentially revealing important ecological trends and
312 interactions between the two environments. We then assess the correlation of the CSI values with
313 changes in temperature, water availability, and coastal OW conditions in the nine sectors and in
314 the Pan-Arctic. This analysis is intended to reveal how changes on said parameters may be driving
315 changes in productivity patterns across the different geographical sectors. From the results of the
316 pairwise plots with regression lines, we identified the key predictors and evaluated their
317 contribution to the variability in CSI. We created a multiple linear regression model and to
318 illustrate its skill, compared the predicted with the observed CSI values.

319

320 Lastly, to investigate the interconnected dynamics of land and ocean GPP and coastal sea ice
321 conditions across the pan-Arctic region, we employ wavelet coherence analysis, using the
322 'WaveletComp' package in R (Rösch & Schmidbauer, 2018). The wavelet technique analyzes
323 periodic phenomena in time series data by decomposing a time series into time-frequency space.
324 It gives information about the dominant modes of variability and how the modes vary in time
325 (Torrence & Compo, 1998). Through wavelet coherence analysis we highlight time periods where
326 two time series co-move at a specific frequency, and can detect if the two series have common
327 cycles. Since the WaveletComp package can only process data without gaps, we use seasonally
328 decomposed missing value imputation for the missing data during non-productive months using
329 the 'imputeTS' package in R (Moritz & Bartz-Beielstein, 2017). This method works well for data
330 with both trend and seasonality. The wavelet and cross-wavelet analysis of land and ocean primary
331 productivity, in conjunction with pan-Arctic OW days, will assess the influence of coastal ice
332 conditions—a unique and significant driver of primary productivity on these adjacent ecosystems.
333 More information on the 'WaveletComp' package can be found in its documentation and the work
334 of Roesch & Schmidbauer (2018).

335

336 **3. Results**

337

338 In terms of the magnitude and timing of peak productivity along the Arctic coastlines, it is observed
339 that across the pan-Arctic, the marine grid cells had a cumulative GPP of 1.25×10^{-5} Pg C yr⁻¹

340 when using the Lewis product, whereas the land grid cells had a total of $3.06 \times 10^{-6} \text{ Pg C yr}^{-1}$. This
 341 indicates that the pan-Arctic coastal marine areas are approximately four (4) times larger or have
 342 300% greater GPP than land when considering data in the last two decades. In terms of timing of
 343 peak productivity, the results in figure 2a show a latitudinal effect in period of peak productivity,
 344 especially in the marine component, with later peaks observed in higher northern latitudes. This is
 345 also seen in the plots in figure 2b where the marine component (blue) is observed to be shifting to
 346 the right with increasing latitude. On land, we see a bimodal distribution with peaks in June and
 347 July. The cumulative frequency distribution plots in figure 2c highlight the divergence of the
 348 timing of peak primary productivity with marine component peaking later in the year. These later
 349 peaks on the ocean side are more pronounced along Eurasian and the CAA coastal zones.

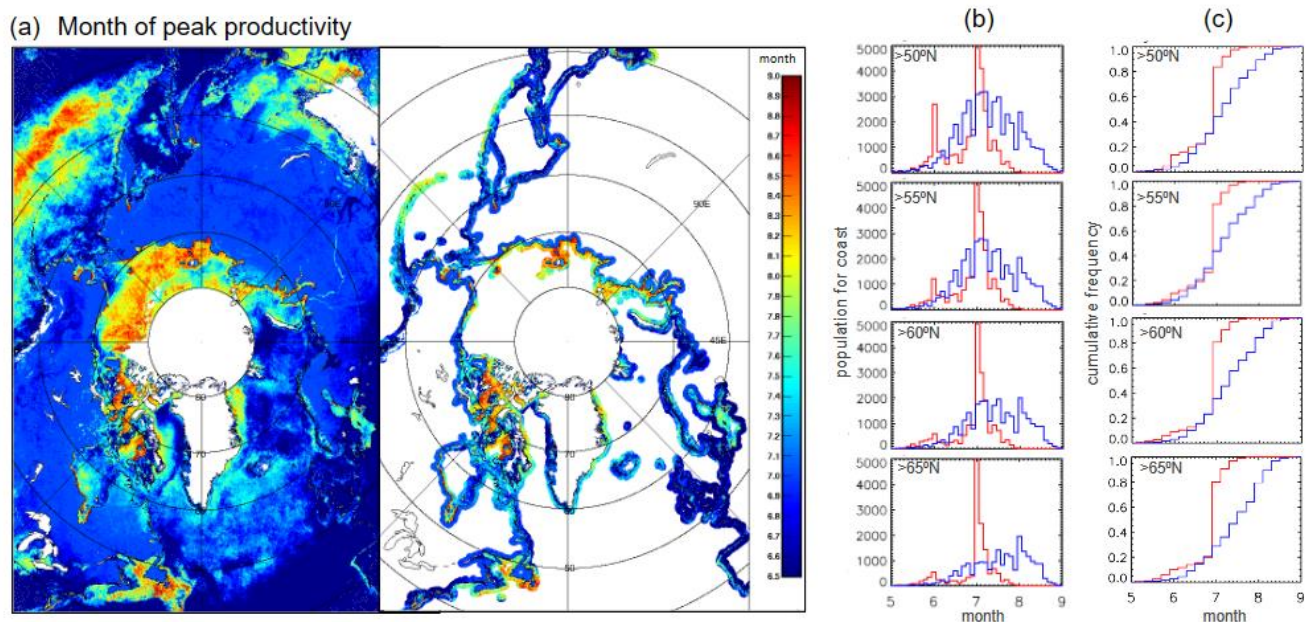
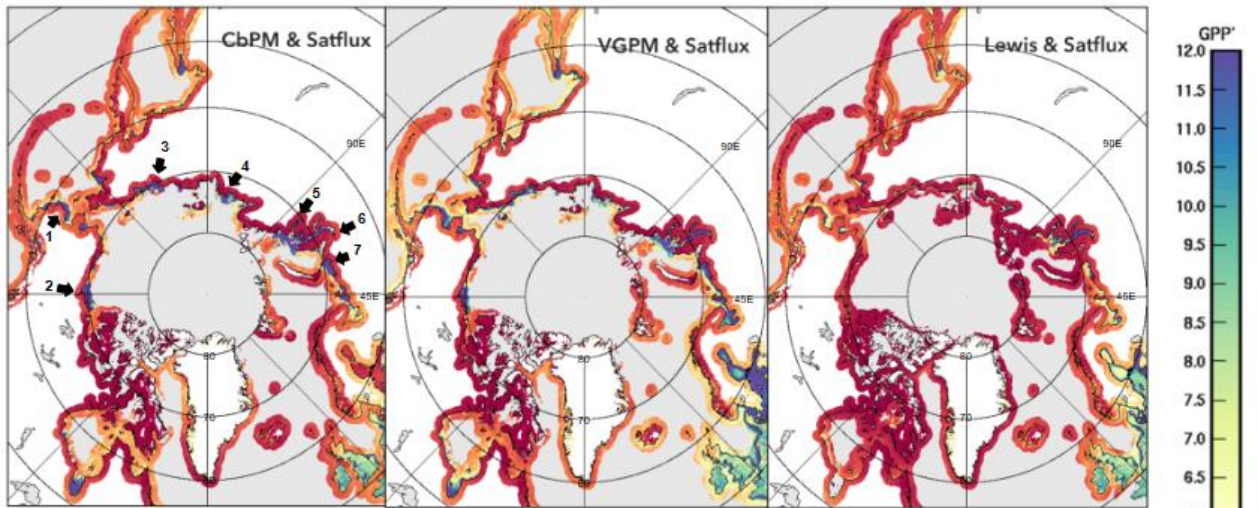


Figure 2. (a) Left panel - map of pan-Arctic peak month productivity on both land and ocean; Right panel - peak month productivity in our study area, 100 km from the coastal margins on land and ocean. (b) Histogram of peak month productivity extracted from >50°N, >55°N, >60°N, and >65°N of the study area. (c) cumulative distribution frequency of peak month productivity from >50°N, >55°N, >60°N, and >65°N of the study area. For both (b) and (c), the blue line corresponds to marine data, while red is for land.

350
 351 In terms of seasonal climatology of coastal productivity, figure 3a shows average data during
 352 spring and early summer (April-June) and summer and early autumn (July-September) in figure
 353 3b for land GPP and the three marine GPP products. High primary productivity is observed along
 354 the mouths of major Arctic rivers (locations are shown in the first panel with black arrows) across
 355 the different marine GPP products. However, a more conservative concentration and distribution
 356 are observed in the Lewis product compared to CbPM and VGPM. The relationship between the

(a) Spring and Early Summer Climatology (April, May, June)



(b) Summer and Early Autumn Climatology (July, August, September)

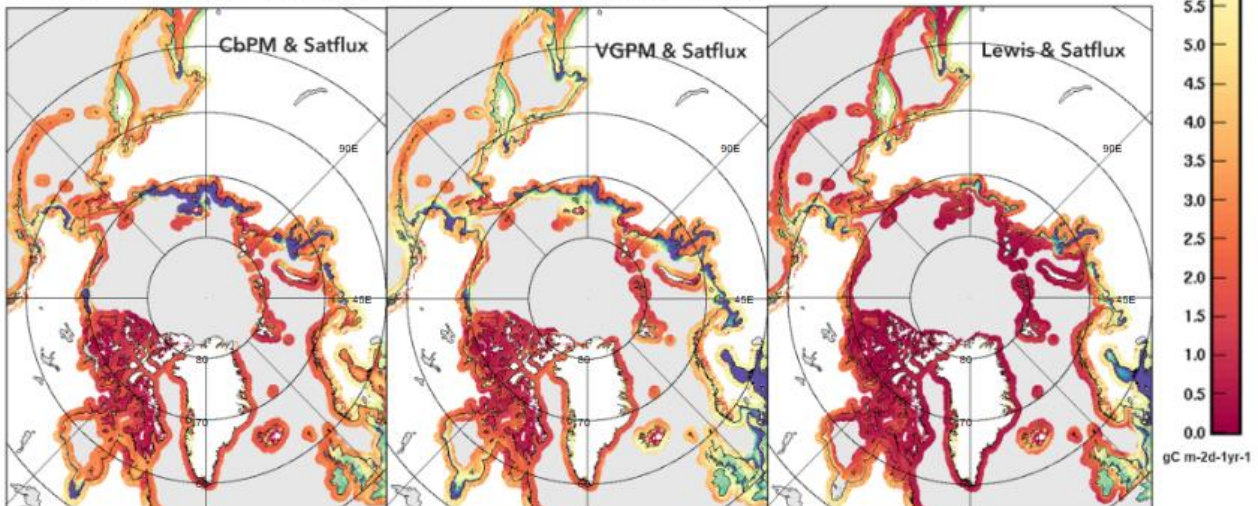


Figure 3. Seasonal climatology of land and ocean primary productivity in the study area. (a) spring and early summer climatology for the months April-June from 2003-2020 for FluxSat land GPP and the three ocean productivity products: CbPM, VGPM, and Lewis. (b) summer and early autumn climatology for the months July-September from 2003-2020 for the same land and ocean primary productivity products. Black arrows on the first panel show the location of the mouths of major Arctic rivers, namely (1) Yukon (2) Mackenzie, (3) Kolyma, (4) Lena, (5) Yenisey, (6) Ob, and (7) Pechora.

357 timing of sea ice melt and marine primary productivity is more evident in figure 3b. At the height
358 of summer and early autumn, sea ice completely disconnects from the shoreline exposing open
359 ocean areas for photosynthesis causing the distinct peaks of GPP. There is also the contribution
360 from the highly seasonal delivery of nutrients from rivers and coastal erosion (Terhaar et al., 2021).
361 The adjacent coastal tundra on -another hand, though modest, shows increasing productivity after
362 snowmelt in spring and early summer. Productivity values then increase towards peak values in
363 July and August. In terms of distribution, the Arctic coastal tundra shows changes in the spatial
364 distribution of vegetation across north-south climate gradients (Raynolds et al., 2019).

Table 1. Total percent change, land and ocean GPP anomaly trends, and coastal trajectory classification in the Pan-Arctic and nine sectors from the 18-year time series (2003-2020). Significant trends ($p < 0.05$) are in bold.

	Land GPP (% change)	Ocean GPP (% change)			Land GPP Trend (gC m ⁻² d ⁻¹)	Ocean GPP Trend (gC m ⁻² d ⁻¹)			Classification
		CbPM	VGPM	Lewis		CbPM	VGPM	Lewis	
Pan-Arctic	12.625	5.766	11.677	11.510	0.010	-0.004	0.065	0.018	SPS
Eurasian	24.944	-16.760	-8.959	27.152	0.015	0.024	0.237	0.027	SPS
Amerasian	38.868	-15.739	-14.226	-20.067	0.011	0.037	0.029	-0.001	TDS
CAA	18.808	3.253	19.304	22.802	0.013	-0.129	0.065	0.034	SPS
Okhotsk	7.886	3.313	31.009	19.894	0.026	-0.009	0.013	0.005	SPS
Bering	15.879	12.634	18.081	9.949	0.021	0.009	0.035	0.026	SPS
Barents	11.327	-1.435	0.315	28.396	0.009	-0.020	0.070	0.036	SPS
Greenland/Iceland	-7.326	22.887	-0.407	4.443	0.005	0.010	0.013	0.006	SPS
Hudson Bay	5.267	-22.154	12.672	10.266	0.002	0.007	-0.001	0.005	SPS
Baffin/Labrador	7.431	-5.885	-11.524	-11.273	-0.002	-0.002	0.009	0.003	MDS

365

366 In terms of primary productivity trajectory and magnitude of change through time, we found that
 367 primary productivity over land has increased by about 13% in the pan-Arctic between 2003 and
 368 2020 with 0.010 gC m⁻² d⁻¹ added each year (Table 1) or 3,650,000 gC km⁻² y⁻¹. Ocean primary
 369 productivity has also increased by a range of about 12% if using the Lewis data and VGPM, and
 370 6% if using CbPM in the pan-Arctic. Rates of change are 0.018 gC m⁻² d⁻¹, 0.065 gC m⁻² d⁻¹ and -
 371 0.004 gC m⁻² d⁻¹ when using Lewis, VGPM, and CbPM respectively, although only Lewis and
 372 VGPM trends are statistically significant. An overall *Synchronized Positive Shift (SPS)* in pan-
 373 Arctic primary productivity was observed when analyzing coastal margins with the VGPM and
 374 Lewis marine data and FluxSat land data. On a regional level, the Eurasian, Canadian Arctic
 375 Archipelago (CAA), Okhotsk, Bering, Amerasian, and Barents sectors showed statistically

376 significant *SPS* patterns on both land and sea when using VGPM and Lewis trends on the ocean
377 component. Although statistical significance was found only on land, the Amerasian sector
378 demonstrated a *Terrestrial Dominant Shift (TDS)* when considering Lewis data.

379

380 A closer look at the rates of primary productivity on land shows that the steepest greening rates
381 are observed along the North Pacific *inflow margins* of Okhotsk ($0.026 \text{ gC m}^{-2} \text{ d}^{-1} \text{ y}^{-1}$) and Bering
382 ($0.021 \text{ gC m}^{-2} \text{ d}^{-1} \text{ y}^{-1}$). This is followed by Eurasia at $0.015 \text{ gC m}^{-2} \text{ d}^{-1} \text{ y}^{-1}$. Other sectors in order of
383 decreasing land GPP rates are CAA at $0.013 \text{ gC m}^{-2} \text{ d}^{-1} \text{ y}^{-1}$, Amerasian at $0.011 \text{ gC m}^{-2} \text{ d}^{-1} \text{ y}^{-1}$,
384 Barents at $0.009 \text{ gC m}^{-2} \text{ d}^{-1} \text{ y}^{-1}$, Greenland/Iceland at $0.005 \text{ gC m}^{-2} \text{ d}^{-1} \text{ y}^{-1}$, and Hudson Bay at 0.002
385 $\text{gC m}^{-2} \text{ d}^{-1} \text{ y}^{-1}$. Baffin/Labrador, which is an *outflow margin*, is experiencing browning on land at a
386 rate of $-0.002 \text{ gC m}^{-2} \text{ d}^{-1} \text{ y}^{-1}$ although this trend is not statistically significant. In terms of percent
387 change, Amerasian has the highest change during the study period at about 39% increase, followed
388 by Eurasian at 25%, CAA at 19%, Bering at 16%, Barents, at 11%, Okhotsk at 8%, B/L at 7%,
389 and Hudson Bay at 5%. The G/I sector is the only sector that displays a decreasing land primary
390 productivity from 2003 to 2020 at -7%. On the ocean side, the CbPM monthly anomaly trends
391 show decreasing productivity, although values are not statistically significant. The Lewis data and
392 VGPM show similar increasing productivity across the pan-Arctic at $0.018 \text{ gC m}^{-2} \text{ d}^{-1} \text{ y}^{-1}$ and 0.065
393 $\text{gC m}^{-2} \text{ d}^{-1} \text{ y}^{-1}$, respectively. For the VGPM data, the steepest statistically significant increase is
394 observed along the Eurasian nearshore margins at a rate of $0.237 \text{ gC m}^{-2} \text{ d}^{-1} \text{ y}^{-1}$, followed by Barents
395 at $0.070 \text{ gC m}^{-2} \text{ d}^{-1} \text{ y}^{-1}$, CAA at $0.065 \text{ gC m}^{-2} \text{ d}^{-1} \text{ y}^{-1}$, Bering at $0.035 \text{ gC m}^{-2} \text{ d}^{-1} \text{ y}^{-1}$, Amerasian at
396 $0.029 \text{ gC m}^{-2} \text{ d}^{-1} \text{ y}^{-1}$ and G/I at $0.013 \text{ gC m}^{-2} \text{ d}^{-1} \text{ y}^{-1}$. For the Lewis data, the steepest statistically
397 significant increase is observed along the Barents nearshore margins at a rate of $0.036 \text{ gC m}^{-2} \text{ d}^{-1}$
398 y^{-1} , followed by CAA at $0.034 \text{ gC m}^{-2} \text{ d}^{-1} \text{ y}^{-1}$, Eurasian at $0.027 \text{ gC m}^{-2} \text{ d}^{-1} \text{ y}^{-1}$, Bering at 0.026 gC
399 $\text{m}^{-2} \text{ d}^{-1} \text{ y}^{-1}$ and Okhotsk at $0.005 \text{ gC m}^{-2} \text{ d}^{-1} \text{ y}^{-1}$. The only coastal marine sector that is showing a
400 negative rate is Amerasian at $-0.001 \text{ gC m}^{-2} \text{ d}^{-1} \text{ y}^{-1}$, though not statistically significant.

401

402 The spatial distribution of Arctic coastal trajectories is highlighted in the GPP trend maps in Figure
403 4. The coastal primary productivity trends in $\text{gC m}^{-2} \text{ d}^{-1} \text{ y}^{-1}$ are shown for marine GPP products,
404 VGPM and Lewis, and land GPP product, FluxSat, with areas with greens showing increasing
405 productivity, and areas with maroons showing decreasing productivity with time. While there are
406 several local-scale “hotspots” present in the data, we focus instead on the sectoral trends and

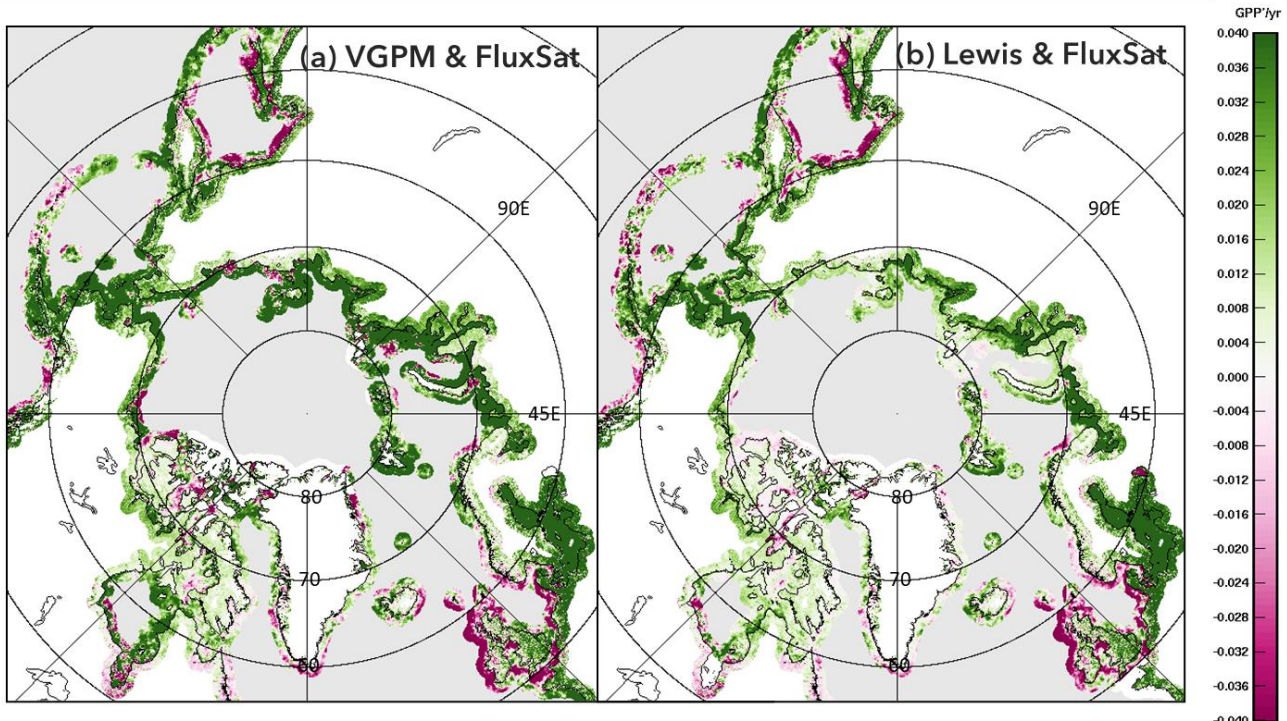


Figure 4. Land and Ocean GPP trends in $\text{gC m}^{-2} \text{d}^{-1} \text{y}^{-1}$ from 100 km from coastline towards land and 100 km towards the ocean from 2003-2020 using (a) VGPM and Fluxsat, and (b) Lewis and FluxSat.

407 regional changes. Figure 4a using VGPM shows some decreasing productivity along some major
 408 river mouths, but also intense blooms (greens) in most sectors. Figure 4b with Lewis data
 409 highlights the convergence, specifically, an *SPS* type of synchrony observed using sectoral trends.
 410 Unlike VGPM, the Lewis trends are more positively conservative. This could be due to the
 411 corrections made by the authors to account for the unique bio-optical conditions of Arctic waters.
 412

413 To explore the potential mechanisms driving the prominent patterns of convergence across the
 414 pan-Arctic coasts, we assess changes in temperature, hydrology, and coastal sea ice conditions.
 415 Table 2 summarizes the monthly anomaly trends in LST ($^{\circ}\text{C yr}^{-1}$), P-E (m yr^{-1}), and Runoff (m yr^{-1})
 416 over land as well as changes in SST ($^{\circ}\text{C yr}^{-1}$), P-E (m yr^{-1}), and OW days (d yr^{-1}) over the ocean.
 417 Also included are the land and ocean (Lewis product) GPP trends in the pan-Arctic and the nine
 418 sectors. Over the almost two decades of data, we observe positive trends in LST at $0.053^{\circ}\text{C yr}^{-1}$,
 419 SST at $0.018^{\circ}\text{C yr}^{-1}$, and P-E over land (0.005 m yr^{-1}) and ocean (0.007 m yr^{-1}). The ice-free
 420 condition in the pan-Arctic is also increasing at 0.152 d yr^{-1} . Statistically significant positive LST
 421 trends occurred in the Eurasian, Okhotsk, and Bering sectors. The steepest positive trend for LST

Table 2. Trajectories of land and ocean productivity in the Pan-Arctic and nine sectors, based on FluxSat and Lewis. Trends of LST, P-E, and Runoff on land, and SST, P-E, OW Days, and Upwelling Favorable Wind Days over the ocean from 2003-2020. Significant trends ($p < 0.05$) are in bold.

	Land GPP Trend	Ocean GPP Trend	Land			Ocean			Upwelling Wind (d yr ⁻¹)
	gC m ⁻² d ⁻¹ yr ⁻¹	gC m ⁻² d ⁻¹ yr ⁻¹	LST (°C yr ⁻¹)	P-E (m yr ⁻¹)	Runoff (m yr ⁻¹)	SST (°C yr ⁻¹)	P-E (m yr ⁻¹)	OW Days (d yr ⁻¹)	
Pan-Arctic	0.010	0.018	0.053	0.005	0.0003	0.018	0.007	0.152	0.0524
Eurasian	0.015	0.027	0.146	0.005	0.006	0.047	0.009	0.291	0.0289
Amerasian	0.011	-0.001	0.039	0.007	-0.007	0.013	0.006	0.114	0.0237
CAA	0.013	0.034	0.051	0.017	-0.003	0.022	0.019	0.005	-0.0005
Okhotsk	0.026	0.005	0.047	0.009	-0.003	0.035	0.012	0.042	0.0213
Bering	0.021	0.026	0.069	0.012	0.006	0.047	0.008	0.084	0.0306
Barents	0.009	0.036	0.044	0.009	0.013	0.036	0.011	0.263	0.0218
Greenland/Iceland	0.005	0.006	-0.017	0.017	0.002	0.001	0.018	0.080	-0.1133
Hudson Bay	0.002	0.005	0.0003	-0.010	-0.012	-0.001	-0.004	0.019	0.13534
Baffin/Labrador	-0.002	0.003	0.005	-0.008	-0.008	-0.012	-0.005	-0.005	-0.0863

422 is found in the Eurasian (0.146 °C yr⁻¹), followed by Bering (0.069 °C yr⁻¹) and Okhotsk (0.047
423 °C yr⁻¹). For SST, statistically significant increases are observed along the Eurasian, CAA,
424 Okhotsk, Bering, and Barents sectors. The steepest statistically significant SST trends are observed
425 along Bering and Eurasian both at 0.047 °C yr⁻¹, followed by Barents (0.036 °C yr⁻¹) and Okhotsk
426 (0.035 °C yr⁻¹). For P-E over both land and ocean, we observe increasing trends, except along
427 Hudson Bay and Baffin/Labrador sectors. In terms of runoff, statistically significant trends are
428 observed along Barents (0.013 m yr⁻¹) and Hudson Bay (-0.012 m yr⁻¹). For upwelling favorable
429 winds, a general increase in days when winds blow parallel to the coast is observed in the pan-
430 Arctic (0.052 d yr⁻¹). Trends in decreasing order are observed along Bering (0.031 d yr⁻¹), Eurasian
431 (0.029 d yr⁻¹), Amerasian (0.052 d yr⁻¹), Barents (0.022 d yr⁻¹), and Okhotsk (0.021 d yr⁻¹).

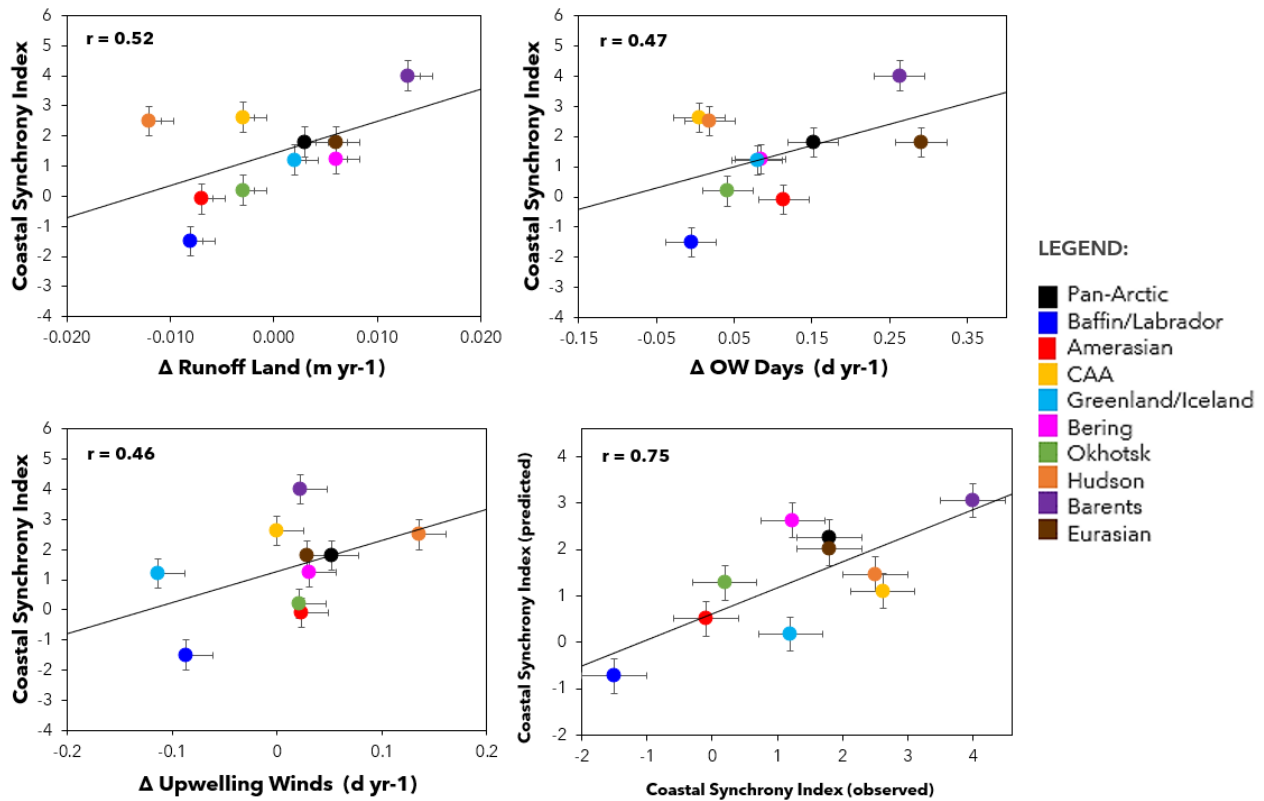


Figure 5. Relationship of changes in Runoff (m yr⁻¹), Open Water (OW) days (d yr⁻¹), Upwelling favorable wind days (d yr⁻¹) vs Coastal Synchrony Index (CSI) based on FluxSat and Lewis data in the pan-Arctic and nine sectors. Error bars are confidence limits on the mean based on bootstrap resampling. The bottom right figure shows observed values of CSI vs predicted values of CSI using a multi-linear regression model including runoff, OW days, and Upwelling wind days as drivers.

432 Interestingly, G/I sector is experiencing decreasing upwelling favorable wind days at -0.113 d yr⁻¹
 433 ¹. Lastly, positive trends in OW days occurred in all regions except in the Baffin/Labrador sector.
 434 The steepest statistically significant increase in open water conditions can be seen in the Eurasian
 435 coastal margin (0.291 d yr⁻¹), followed by Barents (0.263 d yr⁻¹), Amerasian (0.114 d yr⁻¹), Bering
 436 (0.084 d yr⁻¹), Greenland/Iceland (0.080 d yr⁻¹), Okhotsk (0.042 d yr⁻¹), and CAA (0.005 d yr⁻¹).
 437 Overall, we observe a general warming trend on both land and ocean, increasing water availability
 438 through a positive P-E, and a decreasing sea ice condition across the pan-Arctic coastal margins.
 439
 440 When comparing the CSI with changes in other parameters, we find that changes in runoff, OW
 441 days, and upwelling favorable wind days all have explanatory power with respect to the spatial
 442 (i.e., basin to basin) CSI values. To compute the CSI values in these plots, we used the monthly
 443 anomaly trends of FluxSat and Lewis products because the Lewis product was developed as an
 444 Arctic-specific algorithm to help improve estimates of chlorophyll-a, colored dissolved organic
 445 matter (cDOM) absorption, and particle backscattering in the Arctic Ocean (Lewis & Arrigo,

446 2020). As illustrated in figure 5, increasing rates of runoff, OW days, and upwelling favorable
 447 wind days are positively correlated with the ratio of change in ocean and land productivity. This
 448 indicates that the coastal productivity in the ocean is responding faster than land to the increase in
 449 OW days, upwelling wind days, and runoff. Sectors with CSI values greater than 1, namely Barents
 450 (4.0), CAA (2.6), Hudson (2.5), Eurasian (1.8), Bering (1.2), G/I (1.2), and Okhotsk (0.19) suggest
 451 that ocean productivity is changing at a faster rate than land productivity in these coastal areas,
 452 while also displaying a *Synchronized Positive Shift (SPS)* type of coastal productivity trajectory.
 453 Amerasian (-0.09) and B/L (-1.5) sectors have CSI values less than 1, which indicates that ocean
 454 productivity is changing at a slower rate than land productivity in these areas. The pan-Arctic has
 455 a CSI value of 1.8 suggesting that ocean primary productivity might be changing faster than land
 456 and that the two systems are significantly influenced by disappearing coastal sea ice, increasing
 457 upwelling favorable wind days, and transport of water over land. Employing a multiple linear
 458 regression model including runoff, OW days, and upwelling favorable wind days we could explain
 459 approximately 76% of the basin-to-basin variations in CSI.

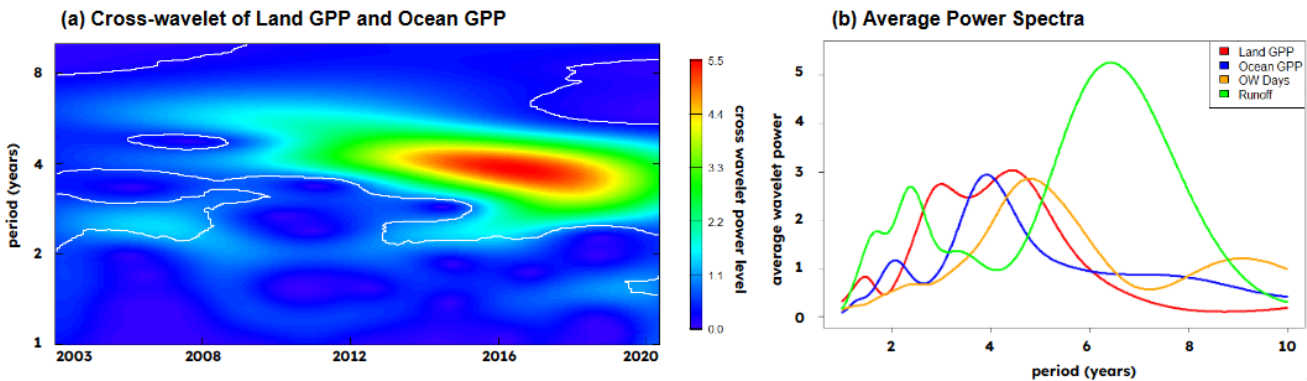


Figure 6. (a) Cross-wavelet transformation of land GPP and ocean GPP in the pan-Arctic using FluxSat and Lewis. White contours represent regions where the observed patterns are statistically significant at the 2.5% level; and (b) Wavelet power spectra of land GPP (red), ocean GPP (blue), OW days (orange), and runoff (green).

460
 461 Decomposing ocean GPP and land GPP into the time-frequency space and looking at their cross-
 462 wavelet transformation in figure 6a and b shows that the adjacent land-ocean systems share a
 463 common dominant period of 4-5 years. This demonstrates that the synchrony we observed from
 464 previous analysis over decadal timescales is mirrored by synchrony on higher frequency
 465 timescales. The ocean GPP (blue) contains a persistent cycle of about 4 years, while the land GPP
 466 (red) contains a dominant period of 3-5 years. The OW days (orange) on the other hand also show
 467 a dominant period between 4-5 years. This shared 4–5-year period between land and ocean GPP

468 appears to be synchronized with a significant 4-5-year natural oscillation of sea ice in polar areas
469 as also observed by Scafetta & Mazzarella (2015). It is also interesting to note that runoff (green)
470 seems to have a dominant period of 7 years and 2 years. These results could indicate that OW days
471 drive land-ocean GPP synchrony on interannual timescales, while the role of runoff is occurring
472 more strongly over longer timescales.

473

474 **4. Discussion**

475

476 Understanding large-scale changes in GPP is crucial in identifying key patterns and processes that
477 promote or inhibit a region's capacity to act as a carbon sink and its vitality as an ecosystem (e.g.
478 declines in GPP may mark susceptibility to disturbances). On the pan-Arctic scale, sustained
479 transformation to a less frozen state has been shown to increase Arctic open ocean NPP by more
480 than 50% between 1998 and 2018 (Lewis et al., 2020). Local-scale estimates however vary
481 depending on sea ice conditions and changing wind patterns (Manizza et al., 2019). The current
482 projected change of Arctic ocean NPP also has a large range, going from a reduction of -25% to
483 an increase of 60% (Vancoppenole et al., 2013) making the determination of not only the amplitude
484 but even the sign of change uncertain. In low-stature coastal tundra environments, vegetation also
485 displays spatially and temporally variable patterns of greening and browning (Frost et al., 2020;
486 Bhatt et al., 2010; Epstein et al., 2018; Stow et al., 2004). Along the coastal regions, which are
487 areas that provide a disproportionate contribution to the global and regional- primary production
488 and carbon storage (Chen & Borges, 2009; Muller-Karger et al., 2005), changes and trajectories
489 of the total photosynthetic CO₂ fixation are quite unknown due to the dearth of studies that consider
490 the marine and terrestrial systems simultaneously. Here we leveraged almost two decades of
491 remotely sensed primary production measurements targeted along the Arctic coastal margins to
492 understand shared spatial and temporal patterns across adjacent terrestrial and marine domains.
493 These are areas of some of the most biologically and geochemically active systems on Earth
494 (McNicol et al., 2023).

495

496 The magnitude of primary production in Arctic coastal margins reveals distinctively higher marine
497 productivity, surpassing that of the tundra environments by four times. Marine systems,
498 particularly coastal zones, are highly dynamic and can rapidly respond to environmental changes,

499 such as extended periods of sunlight as well as nutrient availability following sea ice melt.
500 Terrestrial systems, in contrast, are often constrained by snow cover, the slow thawing of
501 permafrost and shorter growing seasons (Bhatt et al., 2014). Terrestrial environments in the Arctic
502 are also often characterized by less biodiversity and biomass, with plant communities that are
503 adapted to withstand harsh conditions rather than maximize growth (Post et al., 2009; Reynolds &
504 Tenhunen, 1996; Zimov et al., 2006; Schuur et al., 2008). On the timing, the observation that peak
505 productivity in coastal marine zones occurs later than in coastal land areas further north can be
506 attributed to the timing of ice melt, which control available light (Arrigo et al., 2008), nutrient
507 availability (Tremblay et al., 2015), and temperature effects (Steele, 2004). Some marine primary
508 producers might also require a longer period of favorable conditions to initiate their peak
509 productivity phase (Kahru et al., 2011). The divergence in the period of peak month productivity
510 between adjacent marine and terrestrial regions is most evident in the CAA and Eurasia which
511 could potentially be due to longer-lasting sea ice in these regions relative to other parts of the
512 Arctic (Serreze and Stroeve, 2015) as well as from water column stability influenced by river
513 runoff. On land, the bimodal distribution with peaks in June and July shows the shifting of
514 vegetation from early blooming species to those that flourish in the warmer, later parts of the
515 summer (Zhang et al., 2013). For example, dwarf shrubs and sedges peak early in the season, while
516 graminoids and forbs continue to photosynthesize into the late summer, leading to this bimodal
517 pattern. This shift can be indicative of the adaptations and phenological shifts occurring in response
518 to changing climatic conditions (Post et al., 2009). While marine systems may show higher primary
519 productivity levels as well as later and longer peak conditions compared to land, it is important to
520 note that the two systems are closely interconnected. Changes in one can influence the other,
521 particularly in a rapidly warming Arctic. Furthermore, an essential facet of the timing pertains to
522 its implications for observed seasonal cycles of atmospheric CO₂. Regions that synchronize
523 terrestrial and marine productivity might experience short yet intense intervals of CO₂ drawdown
524 (Berkelhammer, 2019). Conversely, regions with disjointed land-sea productivity peaks might
525 display an extended yet less pronounced CO₂ drawdown. Understanding these nuances in both the
526 timing and magnitude of marine and terrestrial GPP is useful, especially when interpreting long-
527 term CO₂ records from monitoring stations like in Utqiagvik (formerly known as Barrow), Alaska
528 and Alert, Canada.

529

530 Assessing the potential
 531 mechanisms behind the observed
 532 convergence and increasing
 533 primary productivity over land
 534 (13%) and ocean (12% and 6%)
 535 from 2003 to 2020 across the
 536 pan-Arctic coasts highlights a set
 537 of interconnected processes
 538 related to climatic changes. The
 539 phenomena of *Synchronized*
 540 *Positive Shift (SPS)* in both
 541 terrestrial and marine
 542 environments across the Arctic
 543 coasts seem to indicate the
 544 effects of Arctic amplification or
 545 increased regional warming
 546 (Serreze and Barry, 2011). This
 547 dynamic is illustrated in figure 7
 548 which shows a representation of
 549 before (top) and after (bottom)

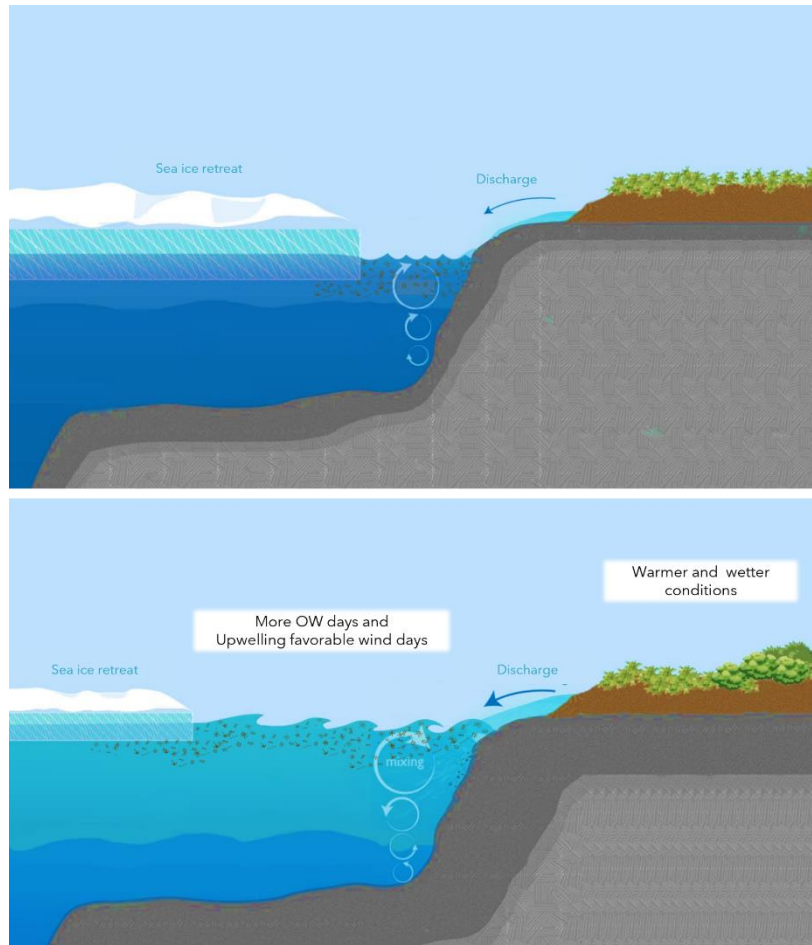


Figure 7. Before (top panel) and after (bottom panel) representation of the Arctic coastal margin as a response to observed warming and increased OW conditions, upwelling favorable wind days, and runoff.

550 observed warming and a corresponding increase in OW conditions, upwelling favorable wind
 551 days, and runoff along the Arctic coasts. In recent years, high OW conditions result in a warmer,
 552 wetter, and more maritime coastal tundra region (Bhatt et al., 2021), which along with earlier
 553 snowmelt positively influences vegetation growth. The observed warming trends, with a positive
 554 change in land surface temperature (LST) of 0.053 °C yr⁻¹ and sea surface temperature (SST) of
 555 0.018 °C yr⁻¹, are conducive to plant growth and phytoplankton blooms, as they often respond to
 556 temperature cues (Thomas et al., 2010; Wassmann et al., 2011). This is particularly evident in the
 557 North Pacific inflow margins of Okhotsk and Bering, which show the steepest greening rates. The
 558 increase in precipitation minus evaporation (P-E) over land (0.005 m yr⁻¹) and ocean (0.007 m yr⁻¹)
 559 indicates greater water availability over land and freshwater in the ocean, further acting to
 560 support productivity. Additionally, the trends towards increased runoff, like the significant

561 increase along Barents (0.013 m yr^{-1}), reflect alterations in regional hydrology that might
562 influence nutrient availability and thus productivity in the ocean and also seems to potentially
563 suggest added water to the landscape is not reducing terrestrial productivity (Peterson et al., 2006).
564 Nutrient availability is also regulated by the interannual variability in riverine, open, and bottom
565 water supply. For our study area, the influence of riverine discharge during spring and summer
566 and the upwelling of nutrients would dominate. Changes in upwelling favorable wind days, with
567 trends observed along Bering (0.031 d yr^{-1}), Eurasian (0.029 d yr^{-1}), Amerasian (0.052 d yr^{-1}),
568 Barents (0.022 d yr^{-1}), and Okhotsk (0.021 d yr^{-1}), may be indicative of alterations in coastal ocean
569 dynamics affecting productivity (Carmack and Chapman, 2003). The increase in open water days,
570 particularly in regions like the Eurasian coastal margin (0.291 d yr^{-1}), aligns with decreasing sea
571 ice conditions, facilitating more sunlight penetration and thereby boosting marine photosynthesis
572 (Arrigo et al., 2008). The observed increase in marine primary production can also be driven by
573 the continuous supply of nutrients from the Pacific Ocean through the Bering Strait (Popova et al.,
574 2013) and from the North Atlantic to the Barents Sea. Declines in sea ice extent can also potentially
575 increase internal wave energy and erode stratification. Overall, positive trends in LST, SST, P-E,
576 runoff, and upwelling favorable wind days across most sectors have contributed to the increase in
577 productivity, driven by the general warming trend, increasing water availability, and decreasing
578 sea ice conditions (Parkinson, 2014; Bintanja and Selten, 2014).

579

580 The observation of varying Coastal Synchrony Index (CSI) values across different Arctic sectors
581 and its relationship with changing environmental conditions show regional dynamics and
582 ecological interconnections. A sector's position on the scatter diagrams in Figure 5, when viewed
583 in light of the CSI, suggests the balance or imbalance between oceanic and terrestrial productivity
584 in response to specific climatic or oceanographic drivers. For instance, sectors with CSI values
585 exceeding 1 in areas like the Barents (4.0), CAA (2.6), and Hudson (2.5) show regional
586 heterogeneity corresponding to areas with the highest rates of change in OW days, runoff, and
587 upwelling favorable wind days. The Barents Sea has been experiencing a pronounced warming
588 trend leading to increased ice-free conditions, thus favoring marine productivity (Polyakov et al.,
589 2020). However, it is worth noting that LST and SST are interestingly not necessarily the direct
590 predictors of CSI, but rather their impact on state conditions. In the CAA, recent changes include
591 shifts in ocean circulation and water mass characteristics, affecting nutrient availability and ocean

592 GPP (Yamamoto-Kawai et al., 2009). Meanwhile, in the Hudson Bay sector, there has been a
593 marked increase in freshwater runoff, potentially influencing nutrient dynamics, and contributing
594 to changes in ocean productivity (Déry et al., 2005). In contrast, sectors such as Amerasian and
595 B/L, with CSI values below 1, hint at a relatively resilient or slow-changing oceanic system,
596 perhaps due to their ecological, climatic, and geophysical properties that generate more buffering
597 mechanisms. In this study, the CSI metric not only offers a consolidated view of how terrestrial
598 and marine ecosystems interact and are influenced by overarching environmental changes, but it
599 also provides a diagnostic tool for evaluating regional ecosystem shifts.

600

601 Given that the Arctic coastal margins are uniquely and vastly sensitive to the timing and presence
602 or absence of sea ice, we first analyzed the coherence of land and ocean primary productivity with
603 each other as well as with the duration of ice-free conditions in nearshore coastal waters.
604 Decomposing ocean GPP and land GPP into the time-frequency space and looking at their cross-
605 wavelet transformation in figure 6a shows that the adjacent land-ocean systems share a common
606 dominant period of 4-5 years. This demonstrates that the synchrony we observed from previous
607 analysis over decadal timescales is mirrored by synchrony on higher frequency timescales. This is
608 also seen in figure 6b, which illustrates the average power, which gives an indication of the strength
609 of the presence of patterns between land and ocean GPP at different periods (years). The ocean
610 GPP (blue) contains a persistent cycle of about 4 years, while the land GPP (red) contains a
611 dominant period of 3-5 years. The OW days (orange) on the other hand also show a dominant
612 period between 4-5 years. This shared 4–5-year period between land and ocean GPP appears to be
613 synchronized with a significant 4-5-year natural oscillation of sea ice in polar areas as also
614 observed by Scafetta & Mazzarella (2015). It is also interesting to note that runoff (green) seems
615 to have a dominant period of 7 years and 2 years. These results could indicate that OW days drive
616 land-ocean GPP synchrony on interannual timescales, while the role of runoff is occurring more
617 strongly over longer timescales.

618

619 To assess higher frequency dynamics in coastal synchrony potentially masked by the multidecadal
620 trends captured in the CSI, we conducted a wavelet coherence and cross-wavelet analysis on
621 adjacent land and ocean GPP. The shared dominant period of 4-5 years illustrates that the coastal
622 synchrony observed over decadal timescales is mirrored over interannual timescales. Looking at

623 the strength of the cycles of land and ocean GPP and OW days, we see a common 4–5-year period,
624 which could indicate that OW days drive the synchrony of land and ocean GPP over interannual
625 timescales. The emergence of shared 4–5-year oscillatory periods in both ocean and land GPP
626 directly corresponds to inherent sea ice dynamics (Scafetta & Mazzearella, 2015). The strong
627 synchrony on the scale of a 4-5-year cycle shared by the parameters observed here indicates that
628 the growing disappearance of shorefast ice not only strongly influences the convergence on
629 adjacent land and ocean primary productivity, but also shares common long-term periodicities with
630 the coastal carbon sink. Interestingly, average power spectra of runoff with a dominant period of
631 7 years seem to show that its role occurs more strongly over longer timescales.

632

633 This study is constrained by the concurrent availability of data over both land and ocean on the
634 years being compared. In addition, the authors have opted to focus on assessing sectoral patterns
635 of primary productivity trends in this study. We recognize the significance of additional factors
636 like coastal erosion, geological characteristics, river runoff, and nutrients, but consistent data for
637 these variables are either sparse or unavailable for the regions and times of interest and are better
638 studied locally in places with intensive measurement strategies. The infrequency of measurements,
639 both temporally and spatially, makes it challenging to accurately constrain net exchanges in coastal
640 ocean settings. Significant uncertainties are also associated with land-derived fluxes, emphasizing
641 the need to comprehend the intricacy of the nutrient budget in this region, particularly along the
642 land-ocean interface. There is also uncertainty associated with remotely sensed observations along
643 the coastal areas. To address uncertainties from the unique bio-optical properties of Arctic coastal
644 waters, the authors utilized primary productivity data from Lewis et al. (2020), along with the
645 traditional ocean primary productivity products that are currently available. The contrasting trends
646 in different products like VGPM, Lewis, and CbPM presented here underline the importance of
647 using multiple data sources to capture the dynamic and multifaceted nature of primary productivity
648 in the pan-Arctic.

649

650 **5. Conclusions**

651

652 This study leverages nearly two decades of remote sensing data to analyze large-scale changes in
653 primary production in the Arctic coastal margins, revealing an interconnected picture of marine

654 and terrestrial environments. The findings show that marine systems in Arctic coastal areas are
655 distinctively more productive than tundra environments, surpassing them by four times. Over the
656 study period of 2003-2020, we learned that GPP along the coastal land and ocean strip has
657 increased by almost the same magnitude of 12%. This indicates that the land-ocean GPP trends
658 along the pan-Arctic coastal margin tend to have expansive or common responses to recent rapid
659 climate change. When looking at the different sectors, the strength and even direction of these
660 trends, a phenomenon we call *Synchronized Positive Shift (SPS)* was observed, showing
661 convergence, and increasing primary productivity over land and ocean across the pan-Arctic
662 coasts, which seem to be a product of increased regional warming. Overall, positive trends in LST,
663 SST, P-E, runoff, and upwelling favorable wind days across most sectors have contributed to the
664 increase in productivity, driven by the general warming trend, increasing water availability, and
665 decreasing sea ice conditions. We observed that inflow margins like Barents, Bering, and Okhotsk,
666 outflow margins like CAA and Greenland/Iceland, as well as interior margins along Eurasia, are
667 sectors where ocean productivity is increasing faster than land productivity. Additionally, the
668 strong coherence on the scale of 4-5-year cycle shared by marine, terrestrial GPP and OW days
669 observed here indicates that the growing disappearance of shorefast ice influences the convergence
670 on adjacent land and ocean primary productivity. As the Arctic coastal areas continue to transition
671 to an ice-free, warmer, and wetter future, it is uncertain whether this SPS pattern between land and
672 ocean GPP along the coastal margins will continue to occur or whether thresholds will be reached
673 where divergence will begin to emerge. We suggest arguing that it is important to integrate the
674 coastal synchrony information developed here as a tool for climate model validation so we can
675 improve our understanding of future trajectories in the coastal Arctic and all the life that it supports.

676

677 **Open Research**

678 We use FluxSat v2.0 GPP product (Joiner & Yoshida, 2020) over land, which is based on the
679 MCD43C Bidirectional Reflectance Distribution Function (BRDF)-Adjusted reflectance from the
680 Moderate-resolution Imaging Spectroradiometer (MODIS) Terra and Aqua. The GPP product over
681 the ocean is estimated from the Carbon-based Productivity Model (CbPM) Net Primary
682 Productivity (NPP) monthly dataset, which was first described by Behrenfeld et al. (2005) and
683 updated by Westberry et al. (2008). The data products used here are Land Surface Temperature
684 (LST) -from the MODIS Aqua MYD11C3 version 6 data product (Wan et al., 2015) available

685 from doi.org/10.5067/MODIS/MYD11C3.006, Sea Surface Temperature (SST) also from the
686 MODIS-Aqua (NASA OBPG, 2020) from doi.org/10.5067/MODSA-8D9D4. The P-E and runoff
687 over land, P-E over the ocean, and Wind data are from the European Centre for Medium-Range
688 Weather Forecasts (ECMWF) Reanalysis 5 (ERA5) (Muñoz-Sabater, 2019) from
689 doi.org/10.24381/cds.68d2bb30. For the sea ice concentration data, we used the Bootstrap version
690 2 (SB2) sea ice data (Comiso et al., 2017) from the National Snow and Ice Data Center (NSIDC)
691 acquired from doi.org/10.5067/7Q8HCCWS4I0R.

692

693 **References**

694

695 Arrigo, K. R., & van Dijken, G. L. (2004). Annual changes in sea-ice, chlorophyll a, and primary
696 production in the Ross Sea, Antarctica. *Deep Sea Research Part II: Topical Studies in*
697 *Oceanography*, 51(1-3), 117-138.

698 Arrigo, K. R., van Dijken, G., & Pabi, S. (2008). Impact of a shrinking Arctic ice cover on
699 marine primary production. *Geophysical Research Letters*, 35(19).

700 Bakun, A. (1990). Global climate change and intensification of coastal ocean upwelling. *Science*,
701 247(4939), 198-201. [DOI: 10.1126/science.247.4939.198](https://doi.org/10.1126/science.247.4939.198)

702 Barnhard K. R., Overeem, I., Anderson, S. (2014). The effect of changing sea ice on the physical
703 vulnerability of Arctic coasts. *The Cryosphere*, 8, 1777-1799. doi:10.5194/tc-8-1777-2014.

704 Behrenfeld, M.J., & Falkowski, P.G. (1997). A consumer's guide to phytoplankton primary
705 productivity models. *Limnology and Oceanography*, 42(7), 1479-1491.

706 doi:10.4319/lo.1997.42.7.1479.

707 Behrenfeld, M. J., E. Boss, D. A. Siegel, and D. M. Shea (2005), Carbon-based ocean
708 productivity and phytoplankton physiology from space, *Global Biogeochem. Cycles*, 19,
709 GB1006, doi:10.1029/2004GB002299.

710 Berkelhammer, M. (2019). Synchronous Modes of Terrestrial and Marine Productivity in the
711 North Pacific. *Frontiers in Earth Science*, Vol 7., ISSN 2296-6463,

712 DOI:10.3389/feart.2019.00073

713 Bhatt US, Walker DA, Raynolds MK, Bieniek PA, Epstein HE, Comiso JC, Pinzon JE, Tucker
714 CJ, Polyakov IV. (2013). Recent Declines in Warming and Vegetation Greening Trends over
715 Pan-Arctic Tundra. *Remote Sensing*, 5(9):4229-4254. <https://doi.org/10.3390/rs5094229>

716 Bhatt U. S. et al., (2010). Circumpolar Arctic tundra vegetation change is linked to sea ice
717 decline, *Earth Interact.* DOI: 10.1175/2010EI315.1.

718 Bhatt, U. S., Walker, D. A., Raynolds, M. K., Comiso, J. C., Epstein, H. E., Jia, G., ... & Pinzon,
719 J. E. (2014). Circumpolar Arctic tundra vegetation change is linked to sea ice decline. *Earth*
720 *Interactions*, 14(8), 1-20.

721 Bhatt U. S. *et al* (2017). Changing seasonality of panarctic tundra vegetation in relationship to
722 climatic variables *Environ. Res. Lett.* 12.

723 Bhatt U.S. *et al* (2021). Climate drivers of Arctic tundra variability and change using an
724 indicators framework. *Environ. Res. Lett.* 16 055019.

725 Bintanja, R., Selten, F. Future increases in Arctic precipitation linked to local evaporation and
726 sea-ice retreat. *Nature* 509, 479–482 (2014). <https://doi.org/10.1038/nature13259>.

727 Carmack, E. C., Polyakov, I. V., Padman, L., Fer, I., Hunke, E., Hutchings, J., ... & Perovich, D.
728 K. (2015). Toward quantifying the increasing role of oceanic heat in sea ice loss in the new
729 Arctic. *Bulletin of the American Meteorological Society*, 96(12), 2079-2105.

730 Carmack, E. C., et al. (2016), Freshwater and its role in the Arctic Marine System: Sources,
731 disposition, storage, export, and physical and biogeochemical consequences in the Arctic and
732 global oceans, *J. Geophys. Res. Biogeosci.*, 121, doi:10.1002/2015JG003140.

733 Carmack, E.C., D. Barber, J. Christensen, R. Macdonald, B. Rudels, E. Sakshaug (2006).
734 Climate variability and physical forcing of the food webs and the carbon budget on panarctic
735 shelves, *Prog. Oceanogr*, 10.1016/j.pocean.2006.10.005.

736 Carmack, E., Chapman, D.C.,(2003). Wind-driven shelf/basin exchange on an Arctic shelf: The
737 joint roles of ice cover extent and shelf-break bathymetry. *Geophysical Research Letters*, 30(14).

738 Chen, C.-T. A., & Borges, A. V. (2009). Reconciling Opposing Views on Carbon Cycling in the
739 Coastal Ocean: Continental Shelves as Sinks and Near-Shore Ecosystems as Sources of
740 Atmospheric CO₂. *Deep Sea Research Part II: Topical Studies in Oceanography*, 56, 578-590.
741 <https://doi.org/10.1016/j.dsr2.2009.01.001>.

742 Clarke, A., & Gaston, K. J. (2006). Climate, energy and diversity. *Proceedings of the Royal*
743 *Society B: Biological Sciences*, 273(1599), 2257-2266. <https://doi.org/10.1098/rspb.2006.3545>.

744 Clow, G. D., DeGange, A. R., Dirksen, D. V., Zimmerman, C. E. (2011). Climate change
745 considerations, in: *An Evaluation of the Science Needs to Inform Decisions on Outer Continental*
746 *Shelf Energy Development in the Chukchi and Beaufort Seas, Alaska*, edited by: Holland-
747 Bartels, L. and Pierce, B., US Geological Survey Circular 1370, 81–108, 2011.

748 Comiso, J. C., W. N. Meier, and R. Gersten (2017). Variability and trends in the Arctic Sea ice
749 cover: Results from different techniques. *Journal of Geophysical Research:*
750 *Oceans*, 122 (8): 6883-6900 doi:10.1002/2017jc012768.

751 Cury, P., & Roy, C. (1989). Optimal Environmental Window and Pelagic Fish Recruitment
752 Success in Upwelling Areas. *Canadian Journal of Fisheries and Aquatic Sciences*, 46(4), 670–
753 680. doi:10.1139/f89-086.

754 Day, J. J., & Hodges, K. I. (2018). Growing land-sea temperature contrast and the intensification
755 of Arctic cyclones. *Geophysical Research*
756 *Letters*, 45, 3673– 3681. <https://doi.org/10.1029/2018GL077587>

757 Déry, S. J., et al. (2005). Characteristics and trends of river discharge into Hudson, James, and
758 Ungava Bays, 1964–2000. *Journal of Climate*, 18(14), 2540-2557.

759 DeGrandpre, M. D., Körtzinger, A., Send, U., Wallace, D. W. R., and Bellerby, R. G. J. (2006),
760 Uptake and sequestration of atmospheric CO₂ in the Labrador Sea deep convection region,
761 *Geophys. Res. Lett.*, 33, L21S03, doi:10.1029/2006GL026881.

762 Elmendorf, S.C.; Henry, G.H.R.; Hollister, R.D.; Bjork, R.G.; Bjorkman, A.D.; Callaghan, T.V.;
763 Collier, L.S.; Cooper, E.J.; Cornelissen, J.H.C.; Day, T.A.; et al. (2012). Global assessment of
764 experimental climate warming on tundra vegetation: heterogeneity over space and time. *Ecol.*
765 *Lett*, 15, 164–175.

766 England, M. R., Eisenman, I., Lutsko, N. J. & Wagner, T. J. (2021). The recent emergence of
767 Arctic Amplification. *Geophys. Res. Lett.* 48, e2021GL094086.

768 Epstein, H. E., Bhatt, U. S., Raynolds, M. K., Walker, D. A., Forbes, B. C., Macias-Fauria, M.,
769 Bjerke, J. (2018). Tundra greenness. In: Arctic Report Card 2018. Retrieved from
770 [https://www.arctic.noaa.gov/Report-Card/Report-Card-](https://www.arctic.noaa.gov/Report-Card/Report-Card-2018/ArtMID/7878/ArticleID/777/Tundra-Greenness)
771 [2018/ArtMID/7878/ArticleID/777/Tundra-Greenness](https://www.arctic.noaa.gov/Report-Card/Report-Card-2018/ArtMID/7878/ArticleID/777/Tundra-Greenness).

772 Farquharson, L.M., D.H. Mann, D.K. Swanson, B.M. Jones, R.M. Buzard, J.W. Jordan (2018).
773 Temporal and spatial variability in coastline response to declining sea-ice in northwest Alaska.
774 *Marine Geology*, 404 71-83.

775 Fernandez-Mendez, M., C. Katlein, B. Rabe, M. Nicolaus, I. Peeken, K. Bakker, H. Flores, and
776 A. Boetius, (2015). Photosynthetic production in the central Arctic Ocean during the record sea-
777 ice minimum in 2012. *Biogeosci.*, 12, 3525-3549.

778 Frey, K. E., D. K. Perovich, and B. Light. (2011). The spatial distribution of solar radiation under
779 a melting Arctic sea ice cover. *Geophysical Research Letters* 38, L22501,
780 [doi:10.1029/2011GL049421](https://doi.org/10.1029/2011GL049421).

781 Frost, G. V., R. A. Loehman, L. B. Saperstein, M. J. Macander, P. R. Nelson, D. P. Paradis, and
782 S. M. Natali. (2020). Multi-decadal patterns of vegetation succession after tundra fire on the
783 Yukon-Kuskokwim Delta, Alaska. *Environmental Research Letters*. 15(2): 025003.
784 [DOI:10.1088/1748-9326/ab5f49](https://doi.org/10.1088/1748-9326/ab5f49).

785 Garcia, C., J. C. Comiso, M. Berkelhammer, and L. Stock (2021). Interrelationships of Sea
786 Surface Salinity, Chlorophyll- α Concentration, and Sea Surface Temperature near the Antarctic
787 Ice Edge. *J. Climate*, 34, 6069–6086, <https://doi.org/10.1175/JCLI-D-20-0716.1>.

788 Graham, R. M., L. Cohen, A. A. Petty, L. N. Boisvert, A. Rinke, S. R. Hudson, M. Nicolaus, and
789 M. A. Granskog (2017), Increasing frequency and duration of Arctic winter warming events,
790 *Geophys. Res. Lett.*, 44, [doi:10.1002/2017GL073395](https://doi.org/10.1002/2017GL073395).

791 Harris, P.T., M. Macmillan-Lawler, J. Rupp, E.K. Baker (2014). Geomorphology of the oceans,
792 *Marine Geology*, Volume 352, Pages 4-24, ISSN 0025-3227,
793 <https://doi.org/10.1016/j.margeo.2014.01.011>.

794 Halsey KH, Milligan AJ, Behrenfeld MJ. 2010. Physiological optimization underlies growth
795 rate-independent chlorophyll-specific gross and net primary production. *Photosynthesis*
796 *Research* 103: 125– 137. DOI 10.1007/s11120-009-9526-z.

797 Irrgang, A.M., Bendixen, M., Farquharson, L.M. et al. (2022). Drivers, dynamics and impacts of
798 changing Arctic coasts. *Nat Rev Earth Environ* 3, 39–54. [https://doi.org/10.1038/s43017-021-](https://doi.org/10.1038/s43017-021-00232-1)
799 00232-1

800 Isaksen, K., Nordli, Ø., Ivanov, B. *et al.* (2022). Exceptional warming over the Barents area. *Sci*
801 *Rep* 12, 9371. <https://doi.org/10.1038/s41598-022-13568-5>

802 Jakobsson, M. (2002). Hypsometry and volume of the Arctic Ocean and its constituent seas,
803 *Geochem. Geophys. Geosyst.*, 3(1), doi:10.1029/2001GC000302.

804 Jeong, et al. (2018). Accelerating rates of Arctic carbon cycling revealed by long-term
805 atmospheric CO₂ measurements

806 Joiner, J., & Yoshida, Y. (2020). Satellite-based reflectances capture large fraction of variability
807 in global gross primary production (GPP) at weekly time scales. *Agricultural and Forest*
808 *Meteorology*, 291, 108092.

809 Kahru, M., Brotas, V., Manzano-Sarabia, M., & Mitchell, B. G. (2011). Are phytoplankton
810 blooms occurring earlier in the Arctic? *Global Change Biology*, 17(4), 1733-1739.

811 Kankaanpää, T, Vesterinen, E, Hardwick, B, et al. Parasitoids indicate major climate-induced
812 shifts in arctic communities. *Glob Change*
813 *Biol.* 2020; 26: 6276– 6295. <https://doi.org/10.1111/gcb.15297>.

814 Kim, YH., Min, SK., Gillett, N.P. et al. (2023). Observationally-constrained projections of an
815 ice-free Arctic even under a low emission scenario. *Nat Commun* 14, 3139.
816 <https://doi.org/10.1038/s41467-023-38511-8>

817 Kwok, R. (2002). Sea ice concentration estimates from satellite passive microwave radiometry
818 and openings from SAR ice motion, *Geophys. Res. Lett.*, 29(9), doi:10.1029/2002GL014787.

819 Leu, E., C. J. Mundy, P. Assmy, K. Campbell, T. M. Gabrielsen, M. Gosselin, T. Juul-Pedersen,
820 and R. Gradinger. (2015). Arctic spring awakening - Steering principles behind the phenology of

821 vernal ice algal blooms. *Progress in Oceanography*,
822 <http://dx.doi.org/10.1016/j.pocean.2015.07.012>.

823 Lewis, K. M., & Arrigo, K. R. (2020). Ocean color algorithms for estimating chlorophyll a,
824 CDOM absorption, and particle backscattering in the Arctic Ocean. *Journal of Geophysical*
825 *Research: Oceans*, 125, e2019JC015706. <https://doi.org/10.1029/2019JC015706>

826 Lewis, K. M., G. L. van Dijken, and K. R. Arrigo, 2020: Changes in phytoplankton
827 concentration now drive increased Arctic Ocean primary production. *Science*, 369, 198-202,
828 <https://doi.org/10.1126/science.aay8380>.

829 Liu, Y., J. R. Key, Z. Liu, and X. Wang, and S. J. Vavrus (2012), A cloudier Arctic expected
830 with diminishing sea ice, *Geophys. Res. Lett.*, 39, L05705, doi:10.1029/2012GL051251.

831 Manizza, M., Menemenlis, D., Zhang, H., & Miller, C. E. (2019). Modeling the recent changes
832 in the Arctic Ocean CO₂ sink (2006–2013). *Global Biogeochemical*
833 *Cycles*, 33, 420– 438. <https://doi.org/10.1029/2018GB006070>.

834 McNicol, G., Hood, E., Butman, D. E., Tank, S. E., Giesbrecht, I. J. W., Floyd, W., et al. (2023).
835 Small, coastal temperate rainforest watersheds dominate dissolved organic carbon transport to
836 the northeast Pacific Ocean. *Geophysical Research Letters*, 50, e2023GL103024.
837 <https://doi.org/10.1029/2023GL103024>

838 Muller-Karger, F.E., Varela, R., Thunell, R., Luerssen, R., Hu, C. and Walsh, J.J. (2005). The
839 importance of continental margins in the global carbon cycle. *Geophysical Research Letters* 32:
840 doi: 10.1029/2004GL021346. issn: 0094-8276.

841

842 NASA Ocean Biology Processing Group (OBPG) and R.P. Stumpf. (2012). Distance to Nearest
843 Coastline: 0.01-Degree Grid: Land. Distributed by the Pacific Islands Ocean Observing System
844 (PacIOOS). http://pacioos.org/metadata/dist2coast_1deg_land.html. Accessed 01 January 2021.

845 National Snow & Ice Data Center (September 21, 2020). *Arctic sea ice decline stalls out at*
846 *second lowest minimum*. Retrieved from:
847 <https://nsidc.org/arcticseaicenews/2020/09/?submit=GO&keywords=2022#:~:text=September%2016%2C%202020%20In%20the%20first%20week%20of,second%20lowest%E2%80%94after%202012%E2%80%94in%20the%2042-year%20continuous%20satellite%20record>.

849

850 National Snow & Ice Data Center (2021). Sea Ice Index, Version 3. National Snow and Ice Data
851 Center. doi: 10.7265/N5736NV7

852 NASA MODIS-Aqua Level 3 SST Thermal IR 8-day 9km Daytime v2014.0.
853 doi.org/10.5067/MODSA-8D9D4. PO.DAAC, CA, USA. Dataset accessed: 15 November 2021.

854 Nishioka, J., Mitsudera, H., Yasuda, I., Liu, H., Nakatsuka, T., and Y. N. Volkov. (2014).
855 Biogeochemical and physical processes in the Sea of Okhotsk and the linkage to the Pacific
856 Ocean, *Progress in Oceanography*, Volume 126, Pages 1-7, ISSN 0079-6611,
857 <https://doi.org/10.1016/j.pocean.2014.04.027>.

858 Nummelin, A., Ilicak, M., Li, C., and Smedsrud, L. H. (2016), Consequences of future increased
859 Arctic runoff on Arctic Ocean stratification, circulation, and sea ice cover, *J. Geophys. Res.*
860 *Oceans*, 121, 617– 637, doi:10.1002/2015JC011156.

861 McIlhatten, E. A., Kay, J. E., & L'Ecuyer, T. S. (2020). Arctic clouds and precipitation in the
862 Community Earth System Model version 2. *Journal of Geophysical Research: Atmospheres*,
863 *125*, e2020JD032521. <https://doi.org/10.1029/2020JD032521>.

864 McLaughlin, F.A & E. C. Carmack, (2010). Deepening of the nutricline and chlorophyll
865 maximum in the Canada Basin interior, 2003-2009. *Geophys. Res. Lett.* *37*, L24602.
866 <https://doi.org/10.1029/2010GL045459>.

867 Minke, M., Donner, N., Karpov, N., De Klerk, P., and Joosten, H. (2007). Distribution, diversity,
868 development and dynamics of polygons mires: Examples from Northeast Yakutia (Siberia),
869 *Peatlands Int.*, 1, 36–40.

870 Moritz, S., & Bartz-Beielstein, T. (2017). imputeTS: Time Series Missing Value Imputation in
871 *R. R J.*, 9, 207.

872 Muñoz-Sabater, J. (2019). ERA5-Land monthly averaged data from 1981 to present, Copernicus
873 Climate Change Service (C3S) Climate Data Store (CDS) [data
874 set], <https://doi.org/10.24381/cds.68d2bb30>.

875 Parkinson, C.L., (2014). Spatially mapped reductions in the length of the Arctic sea ice season.
876 *Geophysical Research Letters*, 41(12), pp.4316-4322.

877 Popova, E. E., Yool, A., Coward, A. C., Dupont, F., Deal, C., Elliott, S., Hunke, E., Jin,
878 M., Steele, M., and Zhang, J. (2012), What controls primary production in the Arctic Ocean?
879 Results from an intercomparison of five general circulation models with biogeochemistry, *J.*
880 *Geophys. Res.*, 117, C00D12, doi:10.1029/2011JC007112.

881 Peterson, B.J., McClelland, J., Curry, R., Holmes, R.M., Walsh, J.E., Aagaard, K., (2006).
882 Trajectory shifts in the Arctic and subarctic freshwater cycle. *Science*, 313(5790), pp.1061-1066.

883 Polyakov, I. V., et al. (2020). Greater role for Atlantic inflows on sea-ice loss in the Eurasian
884 Basin of the Arctic Ocean. *Science*, 356(6335), 285-291.

885 Popova, E. E., Yool, A., Aksenov, Y., and Coward, A. C. (2013), Role of advection in Arctic
886 Ocean lower trophic dynamics: A modeling perspective, *J. Geophys. Res.*
887 *Oceans*, 118, 1571– 1586, doi:10.1002/jgrc.20126.

888 Post, E., Bhatt, U. S., Bitz, C. M., Brodie, J. F., Fulton, T. L., Hebblewhite, M., ... & Walker, D.
889 A. (2013). Ecological consequences of sea-ice decline. *Science*, 341(6145), 519-524.

890 Post, E., Forchhammer, M. C., Bret-Harte, M. S., Callaghan, T. V., Christensen, T. R., Elberling,
891 B., & Aastrup, P. (2009). Ecological dynamics across the Arctic associated with recent climate
892 change. *Science*, 325(5946), 1355-1358.

893 Radic, V. & Hock, R. (2010). Regional and global volumes of glaciers derived from statistical
894 upscaling of glacier inventory data. *J. Geophys. Res.* 115 10.1029/2009JF001373.

895 Rantanen, M., Karpechko, A.Y., Lipponen, A. *et al.* (2022) The Arctic has warmed nearly four
896 times faster than the globe since 1979. *Commun Earth Environ* 3, 168.
897 <https://doi.org/10.1038/s43247-022-00498-3>

898 Rawlins, M. A., Steele, M., Holland, M. M., Adam, J. C., Cherry, J. E., Francis, J. A., ... &
899 Peterson, D. L. (2010). Analysis of the Arctic system for freshwater cycle intensification:
900 Observations and expectations. *Journal of Climate*, 23(21), 5715-5737.

901 Raynolds, M.K., D A. Walker, A. Balsler, C. Bay, et al., (2019). A raster version of the
902 Circumpolar Arctic Vegetation Map (CAVM), *Remote Sensing of Environment*, Volume 232,
903 2019, 111297, ISSN 0034-4257, <https://doi.org/10.1016/j.rse.2019.111297>.

904 Reynolds, J. F. & Tenhunen, J. D. 1996: Landscape function and disturbance in Arctic tundra.
905 Ecol. Stud. 120. Berlin: Springer.

906 Rodriguez-Iturbe, I. (2000). Ecohydrology: a hydrologic perspective of climate-soil-vegetation
907 dynamics. *Water Resources Research*, 36(1), 3-9. <https://doi.org/10.1029/1999WR900210>.

908 Rösch, A., & Schmidbauer, H. (2018), WaveletComp: Computational Wavelet Analysis, R
909 Package Version 1.1, <https://CRAN.R-project.org/package=WaveletComp>.

910 Scafetta, N. & A. Mazzeola. (2015). The Arctic and Antarctic Sea Ice Area Index Records
911 versus Measured and Modeled Temperature Data. *Advances in Meteorology*, Vol 2015,
912 481834, <https://doi.org/10.1155/2015/481834>.

913 Schuur, E. A. G., McGuire, A. D., Schädel, C., Grosse, G., Harden, J. W., Hayes, D. J., ... &
914 Natali, S. M. (2015). Climate change and the permafrost carbon feedback. *Nature*, 520(7546),
915 171-179.

916 Schuur, E. A. G., Bockheim, J., Canadell, J. G., Euskirchen, E., Field, C. B., Goryachkin, V.,
917 Hagemann, S., Kuhry, P., Lafleaur, P. M., Lee, H., Mazhitova, G., Nelson, F. E., Rinke, A.,
918 Romanovsky, V. E., Shiklomanov, N., Tarnocai, C., Venevsky, S., Vogel, J. G., and Zimov, S.
919 A., 2008: Vulnerability of permafrost carbon to climate change: implications for the global
920 carbon cycle. *BioScience*, 58: 701–714.

921 Serreze, M. C., Barrett, A. P., Slater, A. G., Woodgate, R. A., Aagaard, K., Lammers, R.
922 B., Steele, M., Moritz, R., Meredith, M., and Lee, C. M. (2006), The large-scale freshwater cycle
923 of the Arctic, *J. Geophys. Res.*, 111, C11010, doi:10.1029/2005JC003424.

924 Serreze, M. C., & Stroeve, J. (2015). Arctic sea ice trends, variability and implications for
925 seasonal ice forecasting. *Philosophical Transactions of the Royal Society A: Mathematical,*
926 *Physical and Engineering Sciences*, 373(2045), 20140159.

927 Serreze, M.C., Barry, R.G., 2011. Processes and impacts of Arctic amplification: A research
928 synthesis. *Global and Planetary Change*, 77(1-2), pp.85-96.

929 Slagstad, D., Ellingsen, I. H., & Wassmann, P. (2011). Evaluating primary and secondary
930 production in an Arctic Ocean void of summer sea ice: An experimental simulation approach.
931 *Progress in Oceanography*, 90(1-4), 117-131.

932 Stow, D.A., A. Hope, D. McGuire, D. Verbyla., et al. (2003). Remote sensing of vegetation and
933 land-cover change in Arctic Tundra Ecosystems. *Remote Sensing of Environment*, 89, 281-308.
934 doi:10.1016/j.rse.2003.10.018.

935 Terhaar, J., Lauerwald, R., Regnier, P. *et al.* Around one third of current Arctic Ocean primary
936 production sustained by rivers and coastal erosion. *Nat Commun* 12, 169 (2021).
937 <https://doi.org/10.1038/s41467-020-20470-z>.

938 Thomas, D.N., Dieckmann, G.S., 2010. Antarctic Sea Ice—a Habitat for Extremophiles. *Science*,
939 295(5555), pp.641-644.

940 Torrence, C., & Compo, G. (1998). A practical guide to wavelet analysis. *Bulletin of the*
941 *American Meteorological Society*, 79, 61–78.

942 Tremblay, J. É., Anderson, L. G., Matrai, P., Coupel, P., Bélanger, S., Michel, C., & Reigstad,
943 M. (2015). Global and regional drivers of nutrient supply, primary production and CO₂
944 drawdown in the changing Arctic Ocean. *Progress in Oceanography*, 139, 171–196.
945 <https://doi.org/10.1016/j.pocean.2015.08.009>

946 Steele, M. (2004). Ocean–sea ice interactions: a review. In *Sea Ice: An Introduction to its*
947 *Physics, Chemistry, Biology and Geology* (pp. 173-205). Blackwell Publishing Ltd.

948 Walker, D.A., Raynolds, M.K., Daniëls, F.J., Einarsson, E., Elvebakk, A., Gould, W.A., Katenin,
949 A.E., Kholod, S.S., Markon, C.J., Melnikov, E.S., Moskalenko, N.G., Talbot, S.S., Yurtsev, B.A.
950 and The other members of the CAVM Team, (2005), The Circumpolar Arctic vegetation map.
951 *Journal of Vegetation Science*, 16: 267-282. <https://doi.org/10.1111/j.1654-1103.2005.tb02365.x>

952 Wan, Z., Hook, S., Hulley, G. (2021). MODIS/Aqua Land Surface Temperature/Emissivity
953 Monthly L3 Global 0.05Deg CMG V061 [Data set]. NASA EOSDIS Land Processes DAAC.
954 Accessed 2022-09-12 from <https://doi.org/10.5067/MODIS/MYD11C3.061>.

955 Ward, N. et al. (2020). Representing the function and sensitivity of coastal interfaces in Earth
956 system models. *Nature Communications* 11: 1–14.

957 Wassmann, P., Duarte, C.M., Agustí, S., Sejr, M.K., (2011). Footprints of climate change in the
958 Arctic marine ecosystem. *Global Change Biology*, 17(2), pp.1235-1249.

- 959 Westberry, T., Behrenfeld, M. J., Siegel, D. A., and Boss, E. (2008), Carbon-based primary
960 productivity modeling with vertically resolved photoacclimation, *Global Biogeochem.*
961 *Cycles*, 22, GB2024, doi:10.1029/2007GB003078.
- 962 Yamamoto-Kawai, M., McLaughlin, F. A., Carmack, E. C., Nishino, S., & Shimada, K. (2009).
963 Aragonite undersaturation in the Arctic Ocean: Effects of ocean acidification and sea ice melt.
964 *Science*, 326(5956), 1098-1100.
- 965 Zhang, J., Spitz, Y. H., Steele, M., Ashjian, C., Campbell, R., Berline, L., & Matrai, P. (2010).
966 Modeling the impact of declining sea ice on the Arctic marine planktonic ecosystem. *Journal of*
967 *Geophysical Research: Oceans*, 115(10), 1–24. <https://doi.org/10.1029/2009JC005387>.
- 968 Zhang, X., Sun, S., Xie, H., Liu, Y., Shao, D., & Qin, B. (2013). Effects of warming on
969 chlorophyll degradation and carbohydrate accumulation of alpine herbaceous species during
970 plant senescence on the Tibetan Plateau. *PLoS One*, 8(9), e77156.
- 971 Zimov, S. A., et al. (2006), Permafrost and the global carbon budget, *Science*, 312, 1612 – 1613